

# **Dynamics of Longitudinal Biomarker Changes in the APP Transgenic Rat Model of AD**

Monica Shin, BSc

Integrated Program in Neuroscience  
McGill University, Montreal, Quebec, Canada  
December 2015

A thesis submitted to McGill University in partial fulfillment of the requirements of  
the degree of Masters of Science

© Monica Shin 2015

# Table of Contents

<b>Abstract</b> .....	1
<b>Résumé</b> .....	2
<b>Acknowledgements</b> .....	3
<b>Preface &amp; Contribution of Authors</b> .....	4
<b>Glossary</b> .....	5
<b>Introduction</b> .....	6
Signature Pathologies .....	6
Etiology .....	7
Amyloidosis Pattern .....	7
Hypometabolism Pattern .....	8
Neurodegeneration Pattern .....	9
Hippocampal Formation/Atrophy .....	9
Amyloid Hypothesis .....	10
Magnetic Resonance Imaging .....	11
Deformation-Based Morphometry .....	12
McGill-R-Thy1-APP Rat Model of AD .....	13
<b>Study Aims and Hypothesis</b> .....	15
Aim/Hypothesis 1 .....	15
Aim/Hypothesis 2 .....	15
Aim/Hypothesis 3 .....	15
<b>Manuscript</b> .....	17
Abstract .....	18
Article .....	19
Introduction .....	19
Methods and Materials .....	22
Results .....	27
Discussion .....	34
Bibliography .....	40

<b>Hippocampal Volumetry Analysis</b> .....	45
Materials and Methods .....	45
Results .....	51
<b>Summary and Significance of the Research</b> .....	54
Summary of Correlation Analysis .....	54
Summary of Volumetry Analysis .....	54
Validity and Significance of Methodology .....	56
Limitations and Improvements .....	56
Future Directions .....	57
<b>Bibliography</b> .....	58

# Abstract

**Introduction:** Region-specific neurodegeneration in response to amyloid plaque deposition is a topic of interest of Alzheimer's disease (AD) research. Localization of vulnerable areas can help in understanding underlying pathophysiological processes of the disease. Here, using in-vivo magnetic resonance imaging (MRI) and positron emission tomography (PET) neuroimaging techniques, we assess the longitudinal change in hippocampal volume, as well as structural alterations when correlated with baseline levels of amyloidosis and hypometabolism in McGill-R-Thy1-APP transgenic (Tg) rat model of AD. **Methods:** In 5 wild-type (Wt) and 9 Tg rats, [ $^{18}\text{F}$ ]FDG-PET and MRI images were collected at baseline (9-11 months) and follow-up (19 months). [ $^{18}\text{F}$ ]NAV4694-PET was collected from 4 WT and 8 Tg rats. First, total intracranial and hippocampal volumes were acquired by manual segmentation method for analysis of changes in the hippocampus. Then, to observe correlation of baseline PET levels with structural MRI changes, seed values obtained from FDG standardized uptake value ratio (SUV<sub>T</sub>) and NAV binding potential parametric (BP<sub>ND</sub>) images of the frontal cortex, hippocampus, somatosensory cortex and the subiculum at baseline, were correlated with longitudinal deformation maps at voxel-level. Resulting t-maps were Random Field Theory corrected for multiple comparisons. Jacobian **deformation field** values of significant clusters of both Tg and Wt groups were plotted against the baseline PET values, and a linear model of interaction between the PET measurements with the group on the deformation maps refined the clusters. **Results:** Normalized hippocampal volume showed 8.02% decrease in Tg rats only at follow-up. Amyloidosis at baseline correlated with the shrinkage of the right somatosensory and entorhinal cortices, while hypometabolism revealed shrinkages of the left insular and primary somatosensory cortices, fimbria of the hippocampus, and the hippocampus. Additionally, the expansion of the left lateral ventricle was observed. **Discussion:** Our results show that amyloid load and hypometabolism at baseline predict spatially distinct structural changes caused by amyloidosis. Moreover, it shows validation of the manual segmentation method when assessing hippocampal volumetry.

# Abstrait

**Introduction :** La dégénération neuronale causé par la déposition des plaques d'amyloïde est un sujet d'intérêt dans l'étude de la maladie d'Alzheimer (AD). Localiser les structures plus vulnérables permet ainsi une meilleure compréhension du processus pathophysiologique de la maladie. Dans l'étude qui suit, nous utilisons l'imagerie par résonance magnétique (MRI) et la tomographie par émission de positrons (PET) pour évaluer les changements longitudinaux du volume de l'hippocampe, ainsi que les altérations structurales corrélés avec la quantité d'amyloïde et d'hypo-métabolisme à la ligne de base chez le modèle de rat McGill-R-Thy1-APP transgénique (Tg) pour AD. **Méthodes :** 5 rats de souche sauvage (WT) et 9 Tg ont été scannés avec [ $^{18}\text{F}$ ]FDG-PET et MRI au point de référence (9 à 11 mois) et au suivi (19 mois). [ $^{18}\text{F}$ ]NAV4694-PET a été également prise chez 4 rats WT et 8 Tg. Pour les analyses, le volume total du crâne et de l'hippocampe a été segmenté manuellement et ainsi calculé. Par la suite, le ratio des fixations normalisés FDG (SUVR) et le potentiel de liaison du NAV ( $\text{BP}_{\text{ND}}$ ) du cortex frontal, de l'hippocampe, du cortex somato-sensoriel et du subiculum au point de référence ont été corrélés avec les analyses de déformation longitudinale du cerveau par voxel, puis ont été corrigés pour comparaisons multiples. Les valeurs jacobéennes des zones significatives sont tracés vs les valeurs de base PET, permettant d'établir un modèle linéaire de l'interaction entre les mesures PET et les cartes de déformations. **Résultats :** Le volume de l'hippocampe normalisé est diminué de 8.02% chez les rats Tg seulement au suivi. La quantité d'amyloïde au point de référence est relié à une perte neuronale dans le cortex somato-sensoriel et entorhinal de droite, alors que l'hypométabolisme au point de référence est relié à la perte neuronale dans l'insula de gauche et le cortex somato-sensoriel primaire, l'hippocampe et le fimbria. **Discussion :** Nos résultats suggèrent que la quantité d'amyloïde et d'hypo-métabolisme au point de référence prédit les régions qui subiront des changements structuraux causés par l'amyloïde. Ainsi, ces résultats confirment la validité de la segmentation manuelle pour mesurer le volume de l'hippocampe.

# Acknowledgements

The completion my research has been possible with the support, guidance and help from my co-workers, friends, and family. Firstly, I would like to express my most sincere gratitude and respect towards Dr. Pedro Rosa-Neto, my principle supervisor, for having the trust in my potential to conduct this study, by accepting me to his wonderful lab. He has organized opportunities for me to attend international conferences for a close-up experience of this field and, he always monitored the progress in my work to provide guidance when needed. I would also like to express my gratitude for both members of my committee, Dr. Serge Gauthier and Dr. Jens Pruessner, for making time to attend my committee meeting and thesis seminar and for suggesting me helpful ideas and assistance in improving my research method. Also, I would like to thank my external advisor, Dr. Cecilia Flores, for offering her valuable feedback into my work. It is important that I thank PET and MRI technicians, Antonio Aliaga and Axel Mathieu, for providing their skills in image acquisition. I also would like to express my greatest appreciations to my co-workers and colleagues at the lab, for helping me with data processing, image analysis, statistical analysis, and interpretation of data. It is important that I mention Vladimir Fonov, Maxime Parent, Min Su Kang, Sulantha Mathotaarachchi, Seqian Wang, Tharick Ali Pascoal, and Andrea Lessa Benedet. Without them, my research would have not been successfully come to completion. I would like to acknowledge the staff members of the McGill Research Center for Studies in Aging, including Silvana Aguzzi, Joannie Gagnon, Margaret de Chazal, Jean Hall, Marisa Ramirez, Tamar Tatigian, Maria Polcaro, and Manon Derasp, who provided a positive work atmosphere and support for all students of the lab. Lastly, I would like to mention my friends and members of my family, who have always been there for me during my deepest struggles. Melanie Hee Seung Yang, Jae Sik Shin, Christina Shin, Jiwon Shin, Erica Ryoo, Jaemin Bae, Younghoon Ji, and Sara Mohades, you have provided tremendous emotional and mental support. I dedicate this thesis to all those whom I have cross paths with, making this experience extremely memorable.

## Preface & Contribution of Authors

The candidate (Monica Shin) functioned as the principal investigator for all aspects of the study design, adapting, and running the tools for neuroimaging processing and analysis, interpreting the findings, and writing the thesis and the manuscript.

The principal investigator, Pedro Rosa-Neto, has been an invaluable mentor, guiding the research with the latest insight on current literature and field knowledge. He also provided critical input and feedback on interpretation of the significance of findings and writing methods. A.Claudio Cuello and members of his lab, Sonia Do Carmo and Simon Allard, provided the McGill-R-Thy1-APP transgenic rats, as well as information on their genotype and date of birth.

Maxime Parent and Min Su Kang were the key members of PET image acquisition and processing, supplying the processed images to be used in my analysis in conjunction with MRI images provided and processed by Axel Mathieu. Vladimir Fonov carried out the deformation-based morphometry to generate Jacobian determinant maps to be used in my correlation analysis. Sulantha Mathotaraachchi and Tharick Ali Pascoal guided the correlation analysis as statistical consultants, and the results were corrected for multiple comparisons with the help of Seqian Wang, who also assisted in the writing procedure of the thesis. Lastly, Serge Gauthier provided guidance and feedback on the design of the research, examining the progress for the duration of the conduction of research.

The co-authors of the manuscript are member of the McGill University Research Center for Studies in Aging, Douglas Mental Health University Institute, Montreal Neurological Institute, and McGill University.

I (Monica Shin), will be a candidate responsible for the scientific quality of the research, the accuracy of the data, and the quality of reporting. The information in the thesis includes all the data for the submission of the manuscript for publication.

# Glossary

A $\beta$  = Beta-amyloid peptides

AD = Alzheimer's disease

APP = Amyloid- $\beta$  Precursor Protein

BP<sub>ND</sub> = Binding potential

CSF = Cerebrospinal fluid

DBM = Deformation-based morphometry

FAD = Familial Alzheimer's disease

FDG = [<sup>18</sup>F]Fluorodeoxyglucose

MAP = Maximum A Posteriori

MCI = Mild cognitive impairment

MRI = Magnetic resonance imaging

NAV = [<sup>18</sup>F]NAV-4694

NFT = Neurofibrillary tangle

PET = Positron Emission Tomography

[<sup>11</sup>C]PIB = Pittsburg compound B

PS-1 = Presenilin-1

PS-2 = Presenilin-2

p-tau = phosphorylated tau

ROI = Region-of-interest

SUV<sub>r</sub> = Standardized uptake value ratio

Tg = Transgenic

Wt = Wild-type

# Introduction

With the aging population, Alzheimer's disease (AD) has become the most common form of dementia, damaging the brain with progressive neurodegeneration (1). Ultimately, these neurodegenerative changes lead to decline in cognition, which is a characteristic of AD (2). Despite all the research and effort being put into the discovery for the ultimate treatment of this disease, there still is not yet a cure or a vaccine. Aside from providing care for the increasing number of AD patients, it is also important to understand the underlying pathologies that distinguish AD from other forms of dementia for early detection and prevention of the disease. Mapping out the different aspects of the disease manifestation will help with the search for a definitive progressive pattern and early diagnosis of the disease, possibly providing targets for pharmaceutical interventions.

## *Signature Pathologies*

AD is a neurodegenerative disorder with multiple neuropathologies, which include amyloid- $\beta$  ( $A\beta$ ) plaques, neurofibrillary tangles (NFT), brain atrophy, neuroinflammation, cell loss and vascular damage (3). Associated with these biological pathologies, behavioural changes are also observed including memory loss, cognitive deficits, and changes in sleeping patterns. Among the numerous pathological markers, the two main underlying characteristics that contribute to the disease characterization are amyloid plaques made up of  $A\beta_{1-42}$  proteins and NFTs made up of hyper-phosphorylated tau proteins.

The amyloid plaques are the best-known pathology of AD. These extracellular aggregates consist of  $A\beta_{1-42}$  proteins that are the products of abnormal cleavage of Amyloid Precursor Protein (APP) by  $\beta$ - and  $\gamma$ - secretases that lead to the production of the neurotoxic form of the  $A\beta$  peptide instead of normal cleavage by  $\alpha$ - and  $\gamma$ -secretases. It has been suggested that an inflammatory process occurs within these plaques, possibly due to cytokines (3). Depositions of these plaques have been shown to originate in the temporal lobe, including the hippocampus (4), and spread from there towards the frontal lobe area.

The second pathology that is characteristic of AD is the tau protein. Tau is a microtubule-associated phosphoprotein (5), which when abnormally hyperphosphorylated, forms insoluble fibrillary aggregates intracellularly, affecting the neuronal structure (3). Paired helical filaments, composed of hyperphosphorylated tau, constitute these NFTs which are often found in the brains of patients with AD.

### *Etiology*

Amyloid plaques build up and progress to AD may be due to deficits in clearance of APP metabolites from the extracellular space. On a non-amyloidogenic pathway, APP is degraded by a subsequent proteolytic action of a  $\alpha$ - and  $\gamma$ -secretases yielding the hydrophilic and soluble APP. However, in a amyloidogenic pathway,  $\beta$ - and  $\gamma$ -secretases cleave APP into  $A\beta_{1-42}$  and other lipophilic and hydrophobic species, leading to aggregation of  $A\beta$  species in the extracellular space in the form of amyloid plaques. Plaques accumulation has been associated with reduced  $A\beta$  clearance.

Rarely head injury or other traumatic experiences throughout the lifetime (6) or hereditarily due to genetic mutations of the patient, which is defined as the “familial” form of AD. Abundant cases of AD are of the late-onset sporadic form, occurring in people without the genetic abnormalities (7).

Familial AD (FAD), consisting of a minor proportion in the incidence of the disease, is caused by mutations in the gene expression of APP, presenilin-1 (PS-1) and presenilin-2 (PS-2) (8). In the case of APP, which is localized on chromosome 21 (9), different types of mutations at codon 717 of the protein leads to differential cleavage as well as overexpression of the protein. As a result, out of the three proteases that cleave APP, which are  $\alpha$ -,  $\beta$ - and  $\gamma$ -secretases, (10) APP now prefers cleavage by the  $\beta$ - and  $\gamma$ - secretases instead of  $\alpha$ - and  $\gamma$ -secretases (11). As a result of this differential cleavage, insoluble  $A\beta_{1-42}$  fragments aggregate to form plaques that deposit in the extracellular matrix of the brain.

## *Amyloidosis Pattern*

Mildly cognitively impaired (MCI) subjects with amyloidosis of the brain that characterize AD are categorized to be in an early stage of AD (12). The  $A\beta_{1-42}$  level in cerebrospinal fluid (CSF) by lumbar puncture and in the brain by positron emission tomography (PET) are validated measures of amyloidosis. They are inversely correlated in the sense that in the brains,  $A\beta$  plaques are accumulating while CSF level of  $A\beta$  level decreases (13). These measurements have been found to correlate with disease progression (14). A previous study by Jack et al. studied the rate of disease progression in a MCI group that was divided into amyloid-positive and amyloid-negative groups depending on a cut-off value of 1.5 from Pittsburgh Compound B (PIB) amyloid imaging ligand. It was found that the amyloid-positive MCI group showed time-to progression rate dependent of hippocampal atrophy while amyloid-positive and -negative combined groups showed dependence on both hippocampal atrophy and  $A\beta_{1-42}$  load, providing proof that level of amyloidosis can predict the disease progression (15).

Imaging techniques using radio-ligands specific for amyloid plaques are used to detect the level of amyloidosis in the brain. The most common ligands used are the PIB and AV45, and neocortical retention of PIB has been found to correlate with degeneration of brain areas including the hippocampus, although the rate is not (16). Previous findings suggest that although amyloidosis and atrophy are correlated, plaque deposition begins earlier and proceeds at a steady rate until it reaches a plateau while atrophy rate accelerates (16). In AD, the amyloid burden seems to occur prior to other characteristic pathologies such as neurodegeneration and cognitive decline. There are other variants of radio-ligands used for detection of amyloid in the brain, and [ $^{18}\text{F}$ ]NAV-4694 is (NAV) one of them. Similar to PIB, it is a ligand with a high sensitivity for amyloid plaques, yielding an image with better contrast than some of the ligands with low sensitivity. NAV, therefore, can be used in generation of positron emission tomography (PET) images with an optimized signal-to-noise ratio to be used in the analysis of AD brains in research (17).

### *Hypometabolism Pattern*

Another imaging technique used in studying AD is the radio-ligand [<sup>18</sup>F]Fluorodeoxyglucose (FDG), which shows brain areas of high metabolism in relation to the intensity of the radioactive signal. In AD, early hypometabolism is observed throughout the brain including the posterior associative cortical areas and prefrontal regions (18).

A research area of interest is linking the area of hypometabolism with regions that display atrophy. In line with other pathophysiological mechanisms, hypometabolism of the posterior cingulate and orbitofrontal cortices have been suggested to relate to hippocampal atrophy. Since the hippocampus is not an independent region but rather a region that is connected to the anterior cingulate, posterior cingulate, the subgenual region many other regions, the result of hippocampal atrophy on metabolic changes in the linked regions is of interest (19).

### *Neurodegeneration Pattern*

Previous longitudinal studies focusing on atrophy patterns in AD brains have shown acceleration of neurodegeneration pattern along with disease progression (20, 21, 22, 23). The decrease in brain volume at certain vulnerable regions is due to several factors including neuronal, glial and neuropil volume loss (24). The result of gray matter atrophy is reflected in the enlargement of ventricular volume, which is used to characterize AD along with hippocampal and other regions that atrophy. There are regions that targeted specifically in AD due to differences in the vulnerability between certain areas. The most well known regions include the hippocampal formation and the entorhinal cortex of the mesial temporal lobe (25). White matter atrophy has also been discovered in the cingulum bundle, fornix, perforant path and frontal and temporal white matter (26).

Although the affected regions have been identified, there are contradicting findings on the time point of the atrophy along the disease manifestation. Several studies have shown hippocampal atrophy around 5.5 years prior, followed by cortical atrophy around 3.5 years prior to clinical diagnosis have been observed in

FAD patients (27, 28), along with the precuneus and posterior cingulate (29). There also have been studies that show absence of significant atrophy in the non-symptomatic carriers of FAD mutation compared to control group in both the hippocampus and the cortical areas of the brain (30).

### *Hippocampal Formation/Atrophy*

The hippocampus is a memory-processing centre of the brain and is vulnerable to damage in the preclinical stages of AD (4). Hippocampal atrophy was also found to be present in some normal elderly subjects in longitudinal studies, whom demonstrated higher risk of developing dementia (31). In FAD, hippocampal atrophy can be observed early on when symptoms are not visible yet, and around 25% atrophy was observed when comparing mildly symptomatic patients against the controls (27). Indeed, the hippocampus is an area that is used as a predictor of disease progression from MCI to AD (32, 33, 34).

The reason behind the targeting of the hippocampus in the disease progression could be explained by the presence of pyramidal neurons in the hippocampus that are affected by age-related degenerative changes (35). Without a doubt, hippocampal formation has a heavy involvement in severe cases of AD, so much that AD has been called a 'hippocampal dementia' (2, 36).

### *Amyloid Hypothesis*

The role of these biomarkers in the etiology of the disease has been a controversial topic for decades. There have been multiple attempts to place the observed morphological and biochemical changes into a temporal sequence of pathogenesis (3). The leading central hypothesis called the "amyloid hypothesis" has been proposed by Hardy and Higgins in 1992, which explains the sequence of the events that occur in the brains of AD patients (37). The basis of this hypothesis is the  $A\beta_{1-42}$  protein, the main component of the extracellular plaques, which serves as the trigger to the other AD manifestations occurring in the brain. The cascade initially is triggered by the increased formation of these toxic forms of  $A\beta_{1-42}$

proteins, which in turn leads to the formation of NFTs. In the long run, it leads to progressive cell loss, vascular damage (38) and atrophy in the brain, accompanied by cognitive decline. The biochemical mechanism that explains the interaction of amyloid plaques with neurofibrillary tangles comes from the finding that A $\beta$  peptides disrupt calcium homeostasis, leading to an increase in the intraneuronal calcium concentration. Since the phosphorylation of tau proteins can be controlled by intracellular calcium that results in hyperphosphorylation and formation of helical filaments (39), this hypothesis links these two pathologies of AD.

A cascade, that agreeably illustrates this hypothesis, has been suggested by Dr. Clifford Jack, in his 'biomarker cascade model'. This model also shows A $\beta$  build-up as the initial trigger that leads to downstream cognitive decline and neurodegeneration. Although A $\beta$  is considered as the critical protein in beginning of the model, it eventually reaches a plateau, and the progression of the disease is defined by the severity of atrophy in the brain. Furthermore, the resulting cognitive decline is also not considered as a direct impact of A $\beta$ , as high levels of A $\beta$  protein does not affect cognition (40). Thus, in collaboration with the biomarker cascade model, the amyloid hypothesis postulates the necessity for primarily altered form of APP followed by causative tangle formation, leading to calcium-mediated neuronal death (37).

### *Magnetic Resonance Imaging*

Application of structural imaging techniques such as Magnetic Resonance Imaging (MRI) allows for assessment of brain structural changes in vivo. It is a non-invasive method that provides anatomical visualization of the human brain structure. Before the use of non-invasive imaging techniques, it was not possible to have a definite diagnosis of AD, and up until the beginning of the 1990s, post-mortem ex-vivo methods involving biopsy or autopsy were used for definitive diagnosis (41, 42). In the 1990s, presence of hippocampal atrophy was often carried out by visual inspection (43) and even previous diagnosis using hippocampal measurements from a single slice has shown failure in segregating controls from AD

group (44, 45). Cross-sectional analysis in brain volume change is possible in post-mortem tissues, but comparison of rates of change of the volumes for longitudinal observations within the same subject is only possible when using in-vivo imaging techniques. The advantage in the use of MRI techniques is especially valuable in the early stages of the disease for prodromal diagnosis for presymptomatic characteristics of the neurodegenerative diseases, including AD (46).

Acquisition of an MRI image involves the usage of different magnetic field strengths and scanning parameters depending on the available machine, the subject to be scanned and the intended gray/white matter contrast. Depending on the desired resulting specifications of the image, it is technical to develop the correct scanning sequence for optimization of the image. Even after scanning, there needs to be preprocessing steps that will improve the image quality through reduction of artifacts (47).

The application of MRI technique will, as a result, provide a 3D volumetric data set to be used for the analysis of changes in brain volume. Using these, correlations can be made with other data such as PET images or memory tasks to identify a trend that relates various disease symptoms. In high resolutions, in combination with validated analysis techniques, these images will provide possibilities for assessment of even miniscule changes occurring in the specific regions of the brain as well as the brain as a whole (48).

### *Deformation Based Morphometry*

The next step in applying the acquired MR images is investigating for structural differences among groups: morphometric analysis. Often, morphometric analyses are essential tools in studying the structural pathology of the human brain in cases of various diseases including AD. There are various approaches; one application of MR images is deformation-based morphometry (DBM) (49).

DBM can be used when localizing statistically different macroscopic neuro-anatomy of population of interest (50). Specifically, DBM is used when comparing voxel-level positional differences of the whole brain compared to a standard brain

(49). In certain cases, it is trivial to quantitatively identify morphometric features, and DBM helps to assess these structural changes in an unbiased way by yielding results of region-by-region comparison as well as deformation fields. The outcome deformation fields contain information on spatial transformation needed to be applied to the brain in order to match the morphometry of the template used (50). Previous studies have confirmed for usefulness and sensitivity of DBM.

### *McGill-R-Thy1-APP: Transgenic Rat Model of AD*

Despite the well-known cascade of AD pathology and high-tech experimental approaches along with on-going research to finding of the appropriate target sites for preventing the disease progression, there still is not yet one particular answer to terminate this disease from manifesting over bodies of the elderly population. Animal models, especially mammals with similar genetic maps as humans, contribute as a helpful research template for further observation of disease characteristics, aiding in better understanding of the different aspects of the disease (1). An advantage of the use of laboratory animal models is the capability of systemically addressing aspects of human aging that would have been difficult to prove, which would be possible by maintaining the animals under controlled conditions, isolating factors that contribute to individual differences. Common models are rodents, such as rats and mice, and these animals expressing AD-like pathology provide a good model for experimental testing of key elements of the disease cascade (37). Although animal models are used to study the progression of AD and formation of amyloid plaques, many lack NFT expression. These models may not be adequate for study of pathology, but perfect for observing the surviving/compensatory reactions of the brain in case of high A $\beta$  expression (8).

For better understanding of the amyloid hypothesis, different strains of transgenic (Tg) rodents expressing a variety of transgene and promoter combinations have been developed. These rats express abundant amyloid deposition and cognitive deficits (51). The effect of amyloidosis on brain atrophy in animal models of AD have been shown in previous researches. For example, an

experiment conducted in London, UK, by Maheswaran and James in 2009 showed that in the context of AD, amyloidosis and gliosis might be expected to result in an atrophic phenotype in mice models of AD expressing mutations in APP and PS-1 (7).

Taking into consideration that rats display a richer behavioural spectrum along with a larger brain size (52), Dr. A. Claudio Cuello and his team generated the McGill-R-Thy1-APP Tg Wistar rat line. These rats are the first Tg rat models showing full amyloid pathology. The expression pattern in this line of rats are caused by a single human APP transgene containing Swedish and Indiana double mutations that result in the production of full amyloid pathology. These rats containing the transgene under the control of the murine thymocyte antigen promoter (Thy1.2) were genotyped to confirm gene expression. Human amyloid proteins are present inside of the neurons of these rats as early as 1 week postnatal and become more clearly expressed by 2-3 months. The extracellular amyloid plaque expression in the brains of these Tg rats can be observed 6 months postnatal starting from the subiculum, and it spreads to the hippocampus by month-13, accompanied by microglial activation and inflammatory reaction. Cortical plaque formation is also initiated at month-13, and it spreads throughout the whole brain by month 20. As a result, the main areas with intense amyloid plaque expression include the cerebral cortex, hippocampus and entorhinal cortex. Vascular amyloidosis is not observed in these rats. In terms of cognition, McGill-R-Thy1-APP rats show hippocampus-dependent behavioral impairment at 3 months, shown by the Morris Water Maze task. The performance of these rats worsens by 13 months, taking more time to find the platform compared to controls (53).

An advantage of the implication of these McGill-R-Thy1-APP rat models is that in case of mutated APP expression along with PS-1 mutation, amyloidosis is accelerated compared to APP mutation alone (7). Also, the hemizygous Tg rats show lowered amyloid and cognitive expression, illustrating a dose-dependent effect of A $\beta$ . (53). Rodents constitute the preclinical research animal models for human diseases; therefore, human neuroimaging applications are also required for rodents. Therefore, we have applied the neuroimaging techniques used in human research in these rats to look for longitudinal changes in the brain.

## Study Aims and Hypothesis

First, we attempted to manually segment the hippocampal formation of the rats at 11-month baseline and 19-month follow-up time points to compare volumetric differences between the Tg and Wt groups. Taking and incorporating multi-modal techniques and materials we have available, we then attempted to correlate longitudinal structural changes occurring in the brains of these McGill-R-Thy1-APP Tg rats with initial baseline FDG- and NAV-PET values of regions known to show hypometabolism or amyloid deposition. By correlating, we will be able to identify structures that are affected by decreased metabolism and increased amyloidosis.

**Aim 1)** To observe for longitudinal changes occurring in the hippocampal volumetric measurements in the brains of Tg rats *in vivo*, in comparison to Wt rats.

**Hypothesis 1)** In accordance to the expected atrophy of the hippocampus in the Tg rats and Jack et al's plot, atrophy will be unlikely to be detected early on at baseline but will be apparent in the follow-up, while the wt rats will not demonstrate atrophic patterns.

**Aim 2)** To better understand the relationship between longitudinal structural changes with baseline amyloidosis occurring in the brain of Tg rats *in vivo*.

**Hypothesis 1)** We predict increasing atrophy in the AD-signature brains regions of older Tg rats along with increase in amyloidosis. The areas of amyloidosis and atrophy probably will not occur in the same regions since amyloidosis is able to cause distant atrophy.

**Aim 3)** To better understand the relationship between longitudinal structural changes with baseline hypometabolism occurring in the brain of Tg rats *in vivo*.

**Hypothesis 2)** We predict increasing atrophy in the AD-signature brain regions of older Tg rats along with decrease in metabolism.

For the purpose of producing the manuscript that is more focused on the correlation analysis, the results of the correlation studies (Aim 2 and Aim 3) are included in the manuscript. The results of the volumetry analysis (Aim 1), will follow after the manuscript in the thesis.

# Manuscript

## **Dynamics of Longitudinal Biomarker Changes in the Transgenic APP Rat Model of AD**

*Monica Shin<sup>1</sup>, Maxime J. Parent<sup>1</sup>, Vladimir S. Fonov<sup>2</sup>, Min Su Kang<sup>1</sup>, Axel Mathieu<sup>3</sup>, Sulantha Mathotaarachchi<sup>1,2</sup>, Seqian Wang<sup>1,2</sup>, Tharick Ali Pascoal<sup>1</sup>, Simon Allard<sup>4</sup>, Sonia Do Carmo<sup>5</sup>, Serge Gauthier<sup>1,6</sup>, A. Claudio Cuello<sup>5</sup> and Pedro Rosa-Neto<sup>1,6</sup>*

<sup>1</sup> McGill University Research Centre for Studies in Aging, Douglas Mental Health University Institute, Montreal, Canada

<sup>2</sup> McConnell Brain Imaging Centre – McGill University, Montreal, QC, Canada

<sup>3</sup> Brain Imaging Centre – Douglas Hospital, Montreal,, Canada,

<sup>4</sup> Johns Hopkins University, Baltimore, MD, USA,

<sup>5</sup> Department of Pharmacology – McGill University, Montreal, QC, Canada,

<sup>6</sup> Department of Neurology and Neurosurgery, McGill Univeristy, Montreal, Canada

Corresponding author: Pedro Rosa-Neto, MD, PhD.

6875 La Salle Blvd - FBC room 3149, Montreal, QC, Canada H4H 1R3

Email: [pedro.rosa@mcgill.ca](mailto:pedro.rosa@mcgill.ca)

Phone: (+1) 514-761-6131 (ext. 3407)

# Abstract

**Introduction:** McGill-R-Thy1-APP transgenic (Tg) rats are the first rat models showing full amyloid pathology. Building on previous findings showing amyloid plaque deposition in many brain regions in the absence of hippocampal cell death, we performed multi-modal experiments involving Magnetic Resonance Imaging (MRI) and Positron Emission Tomography (PET), hypothesizing the predictability of longitudinal structural changes by baseline levels of amyloid and hypometabolism in Tg but not Wild-type (Wt) animals.

**Methods:** From 5 Wt and 9 Tg rats for [ $^{18}\text{F}$ ]FDG and 4 Wt and 8 Tg rats for [ $^{18}\text{F}$ ]NAV4694, baseline and follow-up PET images were created. Using FDG standardized uptake value ratio maps and NAV binding potential parametric images, regional Tg PET values were extracted from the frontal cortex, somatosensory cortex, hippocampus and the subiculum, which were then correlated with the longitudinal MRI deformation maps using a voxel-level linear model to generate a t-statistical images. After multiple comparison correction with Random Field Theory, surviving significant regions were segmented and applied onto deformation images to extract Jacobian eigenvalues from both Tg and Wt groups. Voxel-level general linear model of the PET and the eigenvalues were correlated, and a linear model of interaction between the PET measurements with the group on the deformation maps refined the clusters.

**Results:** Baseline amyloidosis at 9-11 month led to the shrinkage of the right somatosensory and entorhinal cortices, while baseline hypometabolism led to the shrinkage of the left insular and primary somatosensory cortices, fimbria of the hippocampus, and the hippocampus. Additionally, baseline hypometabolism led to the expansion of the left lateral ventricle.

**Conclusion:** Our results show that the baseline amyloidosis and hypometabolism predict distinct regional structural changes that are not simply caused by aging but also by the existence of amyloidosis. Moreover, they illustrate that amyloid partially explains atrophy patterns seen in AD, which are possibly caused by morphological changes occurring at the synapses.

# Article

## Introduction

Amongst many types of neurodegenerative disorders, Alzheimer's disease (AD) has become the most common form of dementia in the aging population (1). It is characterized by a cascade of multiple pathologies that ultimately leads to cognitive impairment (2). Without a definitive cure for this detrimental disease, there remains a need for the discovery of a therapeutic intervention, which will be made possible, first, by understanding the underlying pathological mechanisms of AD. Scientific research mapping out different aspects of this disease will help us distinguish an accurate progressive pattern and an early diagnosis of AD.

A well-known cascade that incorporates the characteristic pathologies of AD has been plotted by Dr. Clifford Jack in his 'biomarker cascade model' (3). This model shows that extracellular amyloid- $\beta$  ( $A\beta$ ) plaque build-up, which is one of the major biomarkers of AD, acts as the initial trigger that leads to downstream expression of another major pathology, hyperphosphorylated tau (p-tau) proteins, that is involved in the formation of intracellular neurofibrillary tangles (NFTs). Following these protein changes, this model shows resulting neurodegeneration, which can be observed by magnetic resonance imaging (MRI) techniques and positron emission tomography (PET) [ $^{18}F$ ]Fluorodeoxyglucose (FDG) hypometabolism, as well as cognitive decline. Although the increasing build-up of  $A\beta$  plaques is considered as a critical aspect in the beginning of this model, when a plateau is reached, the disease progression is led on by the expression of p-tau, followed by the severity of the atrophy in the brain. Thus, cognitive decline is not considered as a direct impact of  $A\beta$  but rather a consequence of collaboration of amyloid and p-tau protein expressions. Along with this cascade model, the amyloid hypothesis, postulated by Hardy, illustrates the necessity for the primarily altered form of amyloid precursor protein (APP), that leads to over-expression of  $A\beta$  proteins, followed by causative NFT formation that eventually leads to neuronal death and other downstream symptoms seen in AD (4).

Studying individual aspects of AD pathology is difficult, especially because in many cases, the disease progression takes decades, and it is complicated and time-consuming to clinically follow-up on a cohort of patients with large enough power. Furthermore, considering differences in the environmental and genetic diversities in humans, focusing on a single disease pathology is merely possible. To overcome these challenges, animal models are often used in research facilities. Animal models with similar genetic maps as humans contribute as a helpful research template for further observation and understanding of disease characteristics (1). The main advantage is the capability to systematically address different aspects of human aging by maintaining the animals in a controlled environment, isolating factors that contribute to individual differences (5). Rodents expressing AD-like pathologies serve as adequate candidate models for testing key elements of the disease cascade (4). Multiple mice and a few rat models of AD have been shown in previous literatures, mostly expressing mutations in both APP and Presenilin - (PS-1) (6) genes, which when mutated, are known to cause familial AD.

Taking into consideration that rats display a richer behavioural spectrum along with a larger brain size than mice (7), Dr. A. Claudio Cuello and his team generated the McGill-R-Thy1-APP transgenic (Tg) Wistar rat line which is the first Tg rat model showing full amyloid pathology. In these rats, a single human APP transgene with Swedish and Indiana double mutations, under the control of a murine thymocyte antigen promoter, leads to the production of amyloid proteins as early as 1 week postnatal. This APP, as a gene responsible for familial cases of AD, leads to extracellular amyloid plaques deposit by 6-month postnatal, starting from the subiculum and spreading to the hippocampus by month-13. The main areas with intense amyloid plaque expressions include the cerebral cortex, the hippocampus and the entorhinal cortex (8). Most of Tg rodent models of AD express both APP and PS-1 gene mutations, which lead to over expression of APP that is not comparable to levels seen in humans. Since the McGill-R-Thy1-APP rats only express APP mutation, amyloid loads in these animals are more alike the levels seen in humans.

In these Tg rats, a few studies focusing on characterizing this model has been published, but a voxel-wise quantitative comparison between the effects of

magnitude of early amyloidosis or hypometabolism on longitudinal atrophy pattern has not yet been studied. Correlation studies, with the aim to unravel the regional distribution of the discrepancy between the pathological processes throughout the brain, can provide useful information on temporal sequencing of different features of the disease. This approach also brings forth the validation of predictive capability of early levels of amyloidosis and metabolism on possible future neurodegeneration. Correlation studies involving multi-modality techniques are useful since at an early prodromal stage of AD, it is especially challenging to solely measure the degree of atrophy, since it superficially resembles the volume loss that is also observed in healthy elderly individuals (9). Therefore, specific biomarkers capable of distinguishing AD from other types of dementia are needed.

Based on existing literatures showing higher rates of grey matter atrophy in human AD brains with higher amyloidosis (10), as well as spatially distinct neurodegeneration associated with A $\beta$  and tau pathologies in preclinical AD (11), we performed a serial multi-modal correlation study with [ $^{18}$ F]NAV-4694 (NAV-), FDG-PET and MRI for the detection of amyloidosis, hypometabolism, and atrophy, respectively. The first aim of this study was to predict and locate brain regions that are vulnerable to progressive atrophy in case of early regional amyloid expression of areas that are known to have high amyloid plaque build-up at baseline of 9-11 months. Referring to previous literature characterizing the pattern of amyloidosis in the McGill-R-Thy1-APP rats, the regions of interest (ROI) were the frontal cortex, hippocampus, somatosensory cortex and the subiculum (8, 12). To quantify longitudinal structural changes at follow-up of 19 months compared to baseline, MRI images were analyzed at voxel-level using deformation-based morphometry (DBM) technique. The DBM maps can be applied in quantifying the magnitude of regional volume change at a voxel level. Secondly, using these ROI seed regions to quantify baseline hypometabolism, we attempted to predict structural changes in areas vulnerable to early decrease in metabolism. When interpreting the NAV-DBM t-statistical maps, the expected relationship was a negative relationship, since the brain volume is predicted to decrease when fibrillar amyloid level increases. On the other hand, when considering at FDG-DBM t-statistical maps, a positive correlation

was expected so that decrease in brain volume follows hypometabolism. With this serial multi-modality image correlation approach, we aim to provide better prognostic information for region-specific neurodegeneration pattern in AD, with sensitivity to different aspects of AD pathologies such as amyloidosis and hypometabolism.

## Methods and Materials

All experimental procedures involved in this study were approved by the McGill Animal Care ethics committee and were carried out following the Canadian Council on Animal Care guidelines. The animals were provided by Dr. A. Claudio Cuello at the department of pharmacology at McGill University in Montreal, Quebec, Canada. Housing for the rats were held at the animal facility of the Douglas Mental Health University Institute with a 12/12h light/darkness cycle.

### *Cohort*

The cohort consisted of medically healthy McGill-R-Thy1-APP Tg and Wild-type (Wt) Wistar rats. Baseline NAV-PET correlation analysis with longitudinal DBM included 4 Tg and 8 Wt rats, while baseline FDG-PET correlation analysis included 5 Tg and 9 Wt rats. The difference in the sample size between the two analyses was due to physical complications, such as brain tumours, that led to exclusion of certain rats in this study.

## MRI ACQUISITION AND PROCESSING

### *General Procedure:*

The image acquisition procedure was performed by the MRI technician on location, in agreement with the policies of the “Animal Care Committee” of McGill University, Montreal, Quebec, Canada.

### *Animal Preparation:*

The rats were initially anesthetized for 5 minutes with 5% isoflurane in the preparation for scanning 10 minutes prior. After, they were secured using a bite-bar and adhesive tape onto the MRI machine and were maintained anesthetized under 2-3% isoflurane for the duration of the scanning process. The amount of anesthesia varied depending on the weight of the rat. For the entire span of the acquisition process, the heart rate and respiration were monitored; the breathing rate was maintained at 25-30/min.

### *MRI Parameters:*

Whole brain anatomical images were acquired on a 7T Bruker 70/30USR Biospect equipped with the BGA-12S gradient/shim set, the 500V/300A gradient power supply upgrade and a Bruker issued 75/40mm <sup>1</sup>H quadrature volumetric coil. The standard Bruker 3D-TrueFISP (Fast Imaging with Steady State Precession) pulse sequence in ParaVision 5.1 was utilized, with 8 different phase advance ( $\Delta\Phi$ ) angles resulting in 8 images. The final image was the root mean square of these 8 images for a total scanning time just over 45 minutes. The RMS composite image was generated using the MINC2 toolbox (<http://www.bic.mni.mcgill.ca/ServicesSoftware/MINC>).

Scanning was performed under the following Fast Imaging with Steady State Precession (FISP) parameters: spin echo sequence TE/TR= 2.5/5.0ms, effective spectral bandwidth= 50kHz, flip angle= 30°, field of view= 3.6 x 3.6 x 3.6 cm, matrix size= 180 x 180 x 180 points, resolution= 200 x 200 x 200  $\mu$ m, number of slices= 180, phase advance arrays= 180°, 0°, 90°, 270°, 45°, 225°, 135°, 315° (2 averages for each angle, acquisition time of 5 minutes and 48 seconds each).

### *Deformation Map Generation*

For the generation of cross-sectional DBM maps, each of the T2-weighted MRI scans was pre-processed by first, de-noising using the adaptive non-local mean algorithm and then by non-uniformity correction algorithm using N4ITK method (14) with the following parameters: 12 mm spline distance, shrink factor of 4,

convergence threshold of 0.0001 and 2000 iterations. Subsequently, linear intensity normalization was done using histogram-matching with an averaged rat anatomical template. Consecutively, a rough non-linear registration to the rat anatomical template was generated using the Elastix registration program with optical manual initialization using anatomical landmarks and B-spline freeform deformation with 3.75mm distance between nodes. Rigid body registration of the subjects into template space was carried out with Elastix program, using subject-specific brain masks generated by transforming brain masks in template space into subject-specific space, applying an inverse non-linear transformation. Finally, a refined non-linear registration between each subject scan and the template was done using ANTs algorithm.

To generate the Jacobian determinants, a non-linear transformation, generated by co-registering the independently processed T2-weighted scans and brain masks in template space using ANTs, was used. Using each subject's non-linear transformation from each baseline and follow-up time points, the logarithm was calculated for each voxel. This step was followed by non-linear warping into the common template space using the non-linear transformation calculated previously from the cross-sectional analysis for the baseline scan. Subsequently, log-Jacobians of different subjects were analyzed in this space using a unified statistical approach (15). Finally, the Jacobian deformation maps were blurred using a Gaussian kernel of 1mm full-width half-maximum.

## PET ACQUISITION AND PROCESSING

Scanning of all animals was done using a CTI Concorde R4 microPET for small animals (CTI, Siemens Medical Solutions, Munich, Germany) located at Montreal Neurological Institute, Montreal, Quebec, Canada. The scanner was equipped with an anesthesia apparatus as well as a monitor for maintaining the animals in a healthy physiological state for the duration of the scan. The anesthesia of choice was isoflurane, which was administered at 5% initially, then reduced and maintained at 2-2.5% with 0.5L/min of oxygen throughout the scanning procedure.

With the nose cone in place for the administration of the anesthesia, the rats were positioned onto the microPET scanner with the brain centered in the field of view.

### *NAV Scans and Imaging Processing*

First, a transmission scan was carried out using a rotating [ $^{57}\text{Co}$ ] point source for 9 minutes. Then, a simultaneous bolus tail-vein injection of the radiotracer was done with the start of a 60-minute emission scan in list mode acquisition. The resulting dynamic images were histogrammed into consecutive time frames with the following increasing durations: 8 frames x 30 seconds, 6 frames x 60 seconds, 5 frames x 120 seconds and 8 frames x 300 seconds, for a total of 27 frames. Obtained images were reconstructed using a *Maximum A Posteriori* (MAP) algorithm and corrected for scatter, attenuation, dead time and decay.

MINC tools were used, again, for the processing and analysis of the images ([www.bic.mni.mcgill.ca/ServicesSoftware](http://www.bic.mni.mcgill.ca/ServicesSoftware)). Voxel-level analysis of NAV images comprised of calculation of Binding Potential ( $\text{BP}_{\text{ND}}$ ) parametric images using the Simplified Reference Tissue Method with the cerebellar grey matter as the reference region (17).

### *FDG Scans and Imaging Processing*

For a uniform [ $^{18}\text{F}$ ] FDG absorption, all rats fasted 12 hours prior to scanning. Upon the preparation of scanning, 11MBq bolus of [ $^{18}\text{F}$ ] FDG was injected through the tail vein of awake animals 50 minutes prior to initiation of the transmission scan. Each scan consisted of a static emission scan for 20 minutes, followed by a transmission scan of 9 minutes. List mode data were framed into a dynamic sequence of  $8 \times 30$  seconds,  $6 \times 60$  seconds,  $5 \times 120$  seconds, and  $8 \times 300$  seconds frames. Obtained images were reconstructed using a MAP algorithm and corrected for scatter, attenuation, dead time and decay. Processing and analysis of the FDG-PET images was carried out using the MINC Tool Kit as well. After the normalization of the tissue-radioactivity images using the pons as a region of reference, Standardized Uptake Value ratio (SUVr) maps were generated.

### *Generation of PET Parametric Images*

For each of both NAV-BP<sub>ND</sub> and FDG-SUV<sub>r</sub> parametric images, first, manual co-registration of the PET images onto their own MRI was carried out using six degrees of freedom (rigid body transformation). Then, they were non-linearly transformed into a standardized rat brain space, followed by blurring with a Gaussian kernel of 2.4mm full-width half-maximum. The regional NAV binding potential and FDG uptake values were obtained from these images by applying masks of the region of interest, which in turn, gave the average of the values from the voxels covered by the masks. The hippocampus and frontal cortex masks were generated by a colleague, whereas the somatosensory cortex and the subiculum masks were generated by myself, referring to Paxino's rat brain atlas as a guide (17).

### **DBM AND PET CORRELATION ANALYSIS**

First level analysis was performed using a linear regression model between the regional FDG and NAV measurements of Tg rats as independent variables and the deformation maps at voxel level as dependent variables. Operation of the script 'glim\_image' between these variables produced t-statistical maps, which showed areas of significant correlation. As for correction regarding multiple comparisons, the Random Field Theory method was used at a threshold of  $p < 0.05$ .

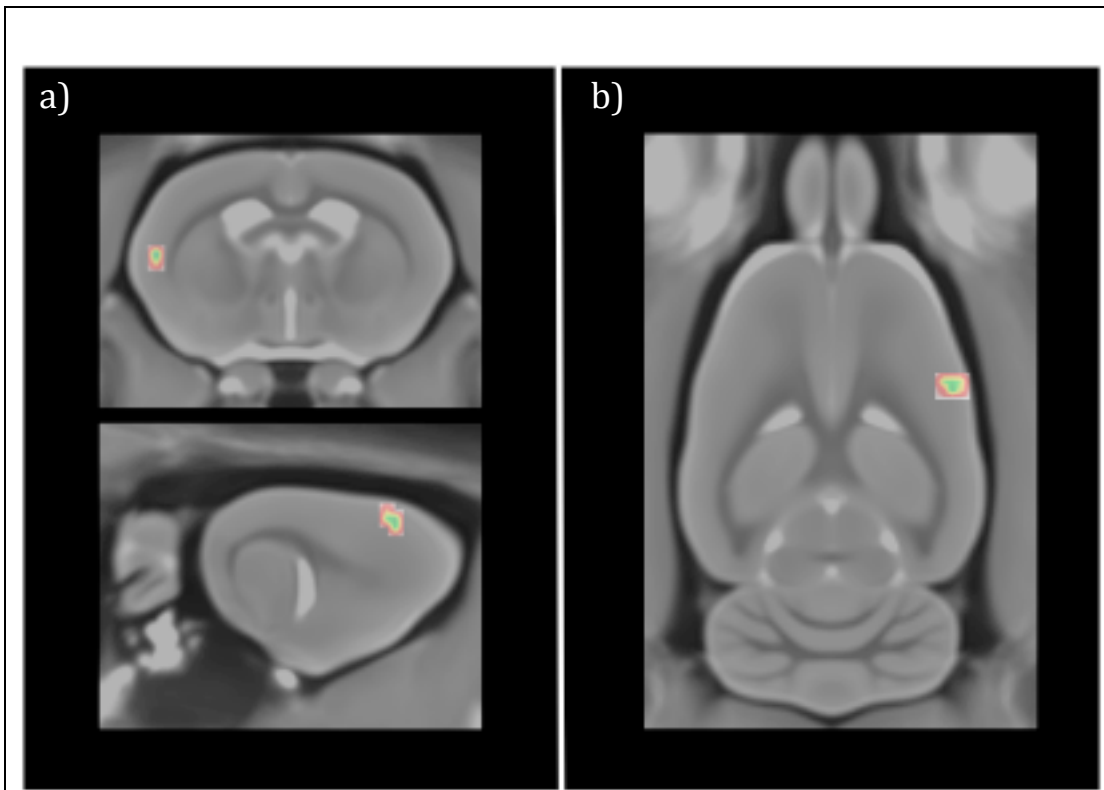
Following this regression analysis, the regions that survived the multiple comparison test were apparent on newly-generated corrected t-statistical maps. Manual segmentation was performed on these significant clusters to generate cluster maps, which were then applied onto the deformation maps for the extraction of Jacobian eigenvalues, representing the amount of deformation required to impose in a grid to match the follow-up to the baseline MRI images. The initial linear regression was implemented on only the Tg group, but the cluster masks were also applied on the Wt rats to extract the Jacobian Eigenvalues of this group as well. Taking these measurements, general linear model analysis was performed with the

PET values of FDG and NAV from each of the respective groups. Lastly, the regression coefficients of the two groups were compared to further aid in refining the clusters, leading to the elimination of results that had comparable coefficients in both groups. As a result, only the correlations that are significant to Tg rats were retained.

## Results

### *Frontal Cortex*

A negative correlation was seen between frontal cortex amyloidosis and the longitudinal deformation map of Tg rats in the left secondary somatosensory cortex (slope coefficient= -1.74,  $R^2= 0.95$ ,  $p<0.0001^{***}$ ) and the right primary somatosensory cortex (slope coefficient= -1.64,  $R^2= 0.99$ ,  $p<0.0001^{***}$ ) (Figure 1). Meanwhile, concerning the frontal cortex hypometabolism, a positive correlation was present in the left insular cortex (slope coefficient= 1.04,  $R^2= 0.91$ ,  $p<0.0001^{***}$ ) (Figure 2).



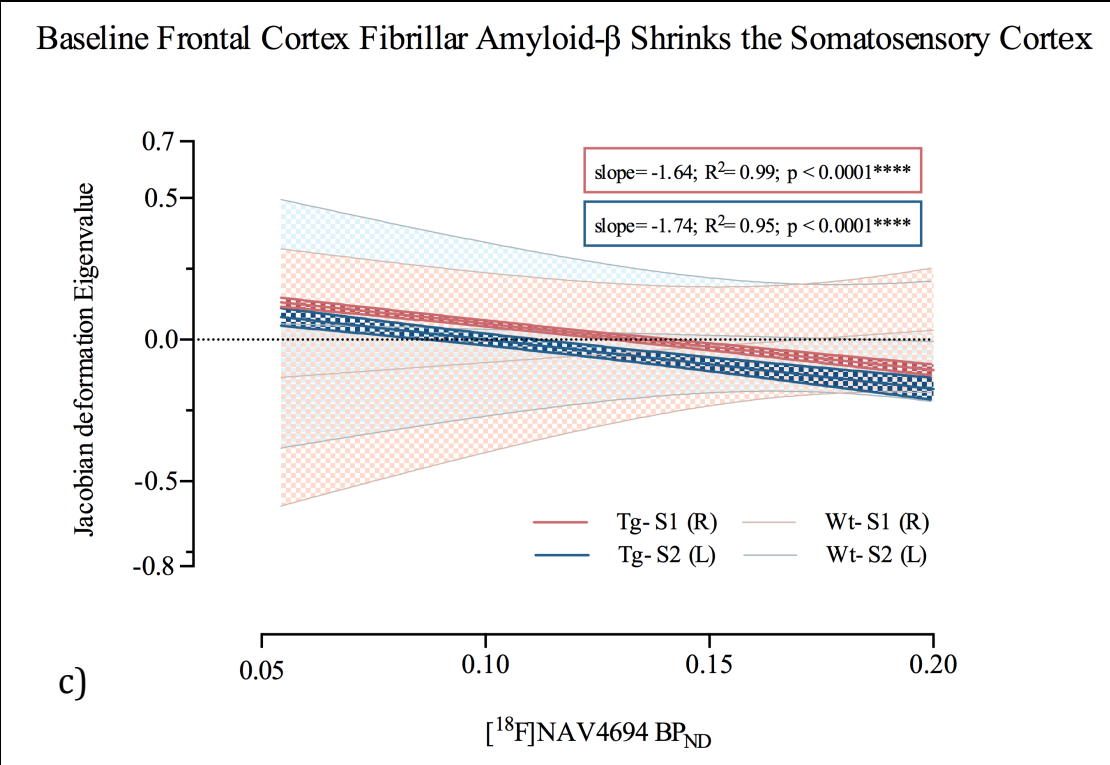


Figure 1. *t*-statistical maps showing regions of significant correlation between frontal cortex NAV seed with longitudinal DBM. The areas correspond to a) left secondary somatosensory cortex and b) right primary somatosensory cortex. c) Graphical representation of frontal cortex NAV correlation with longitudinal deformation changes.

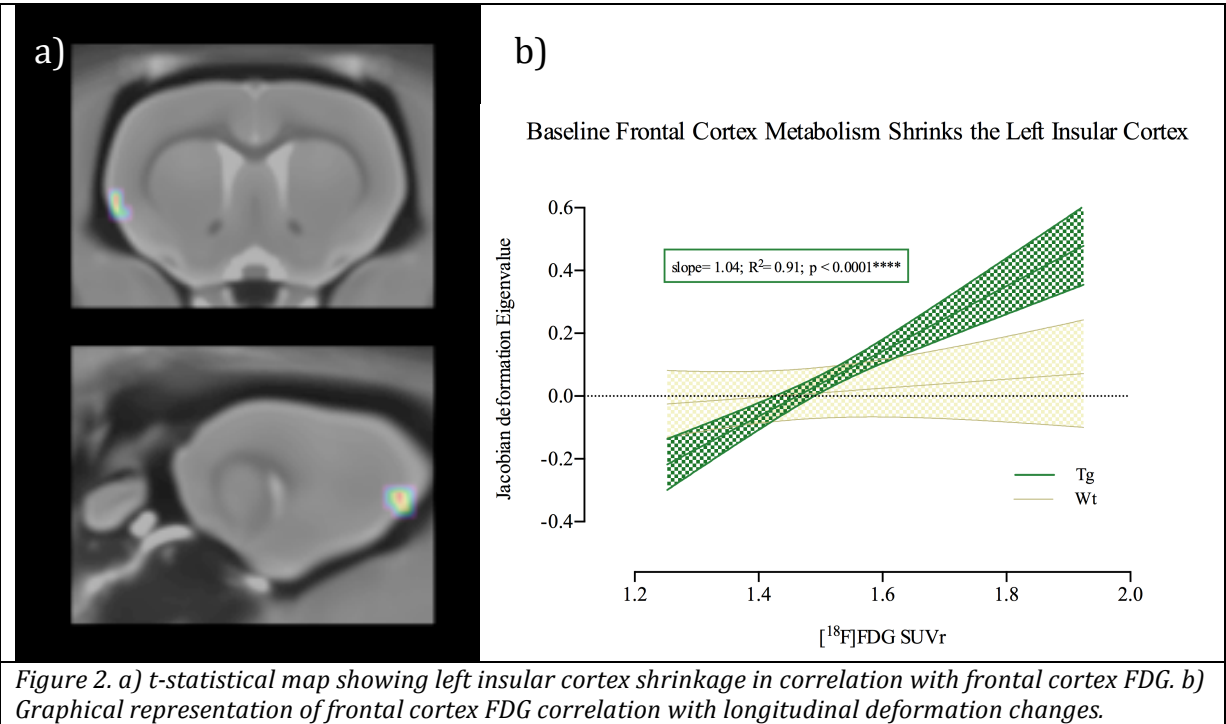
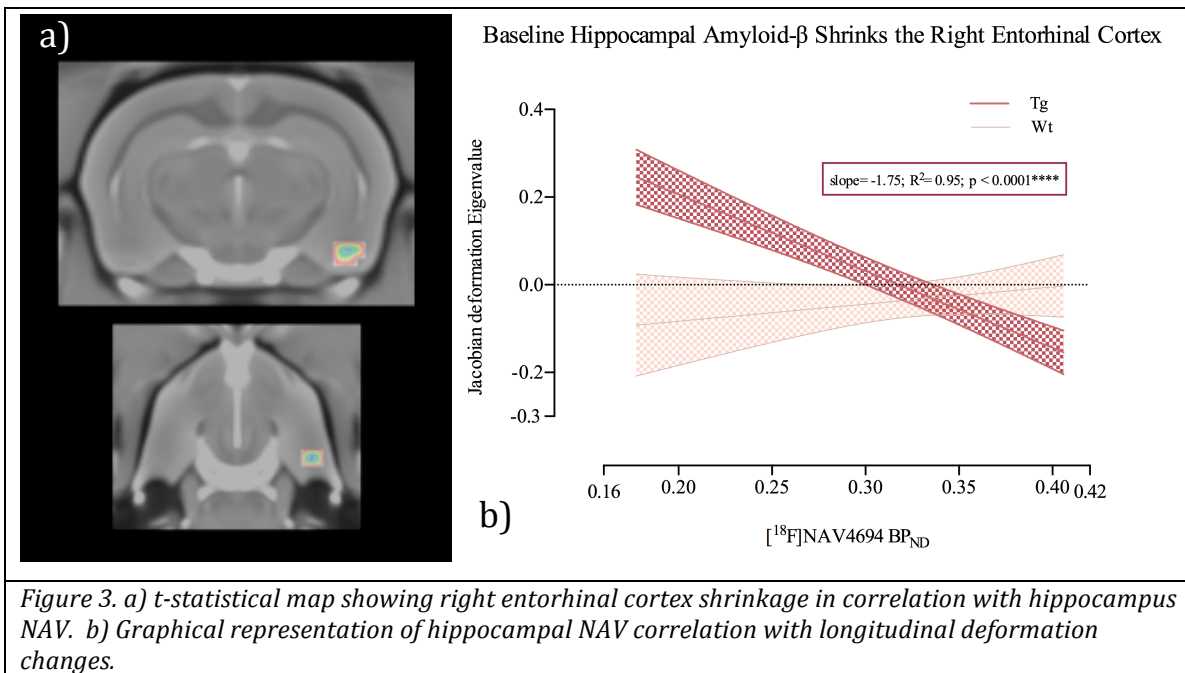


Figure 2. a) *t*-statistical map showing left insular cortex shrinkage in correlation with frontal cortex FDG. b) Graphical representation of frontal cortex FDG correlation with longitudinal deformation changes.

## Hippocampus

The right entorhinal cortex atrophy was found to be correlated with hippocampal amyloidosis (slope coefficient= -1.75,  $R^2= 0.95$ ,  $p<0.0001$ \*\*\*\*) (Figure 3), whereas the left fimbria of the hippocampus (slope coefficient= 0.97,  $R^2= 0.85$ ,  $p=0.0004$ \*\*) and the left somatosensory cortex (slope coefficient= 0.45,  $R^2= 0.87$ ,  $p=0.0002$ \*\*) correlated with the hippocampal hypometabolism. As expected, a desirable negative correlation was also found in the left lateral ventricle (slope coefficient= -0.75,  $R^2= 0.83$ ,  $p=0.0006$ \*\*) (Figure 4).



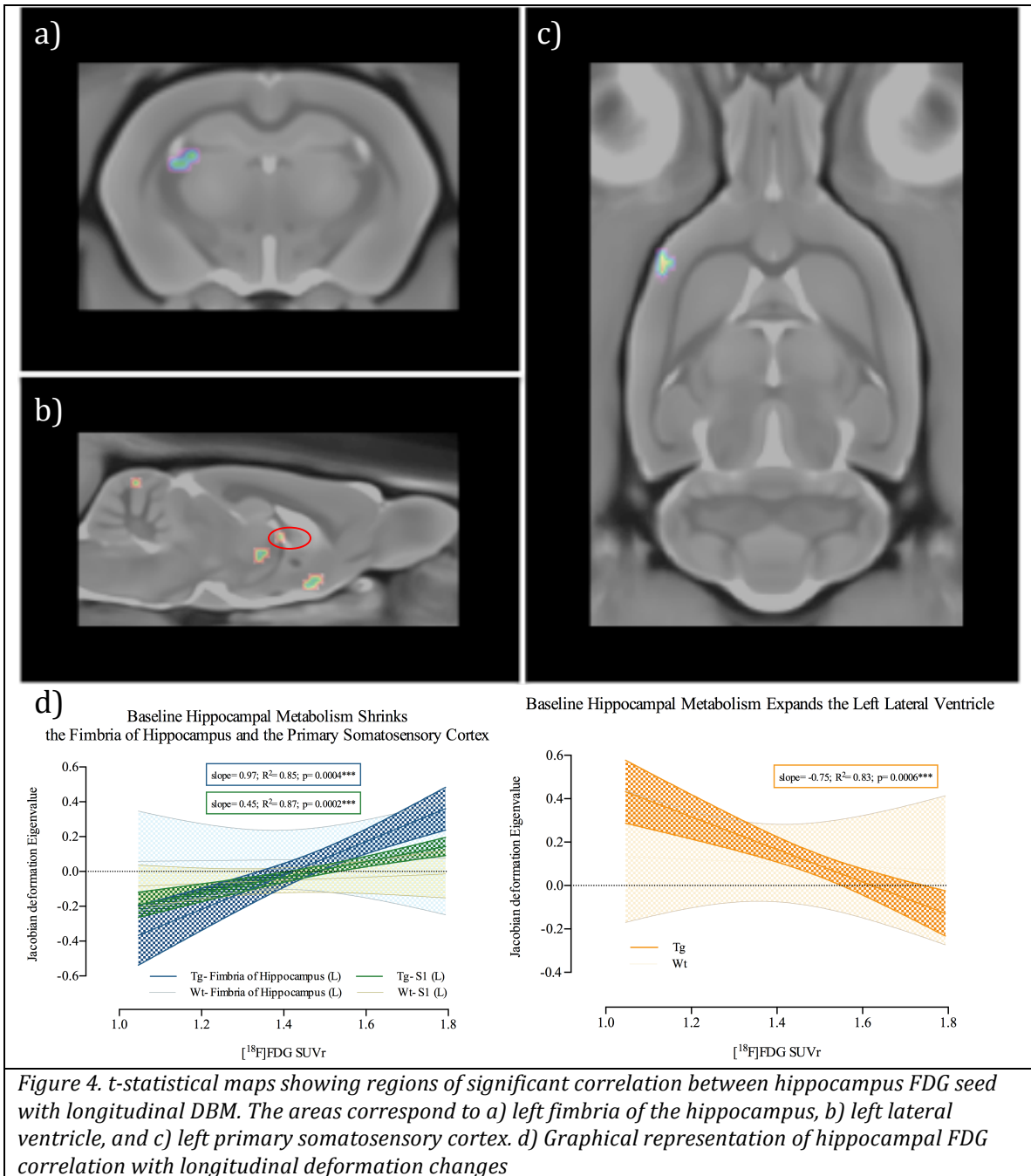
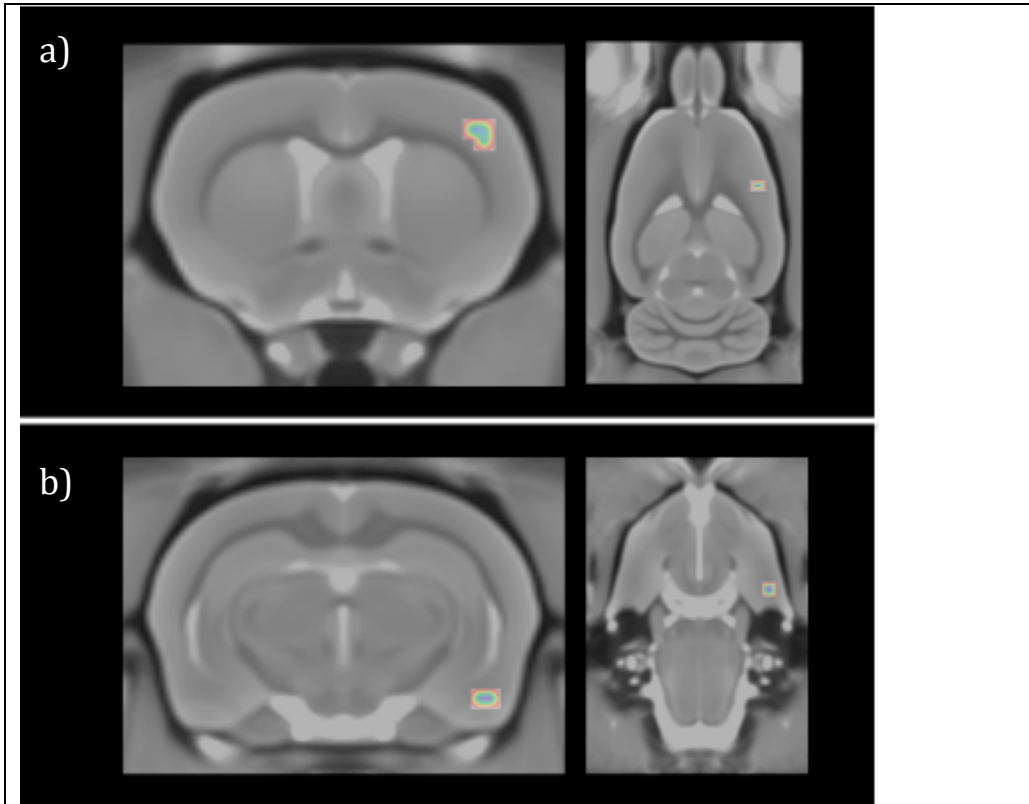


Figure 4. *t*-statistical maps showing regions of significant correlation between hippocampus FDG seed with longitudinal DBM. The areas correspond to a) left fimbria of the hippocampus, b) left lateral ventricle, and c) left primary somatosensory cortex. d) Graphical representation of hippocampal FDG correlation with longitudinal deformation changes

### Somatosensory Cortex

When looking at the somatosensory cortex amyloidosis, regions that showed negative correlation were the right entorhinal cortex (slope coefficient= -1.76,  $R^2=0.90$ ,  $p=0.0004^{***}$ ), which was a region previously seen to correlate with hippocampal amyloidosis, and the right primary somatosensory cortex (slope

coefficient= -1.03,  $R^2= 0.88$ ,  $p=0.0006^{***}$ ) (Figure 5). The left primary somatosensory cortex (slope coefficient= 0.67,  $R^2= 0.89$ ,  $p=0.0001^{***}$ ) and the left hippocampus (slope coefficient= 1.13,  $R^2= 0.91$ ,  $p<0.0001^{***}$ ) positively correlated with the somatosensory cortex hypometabolism (Figure 6).



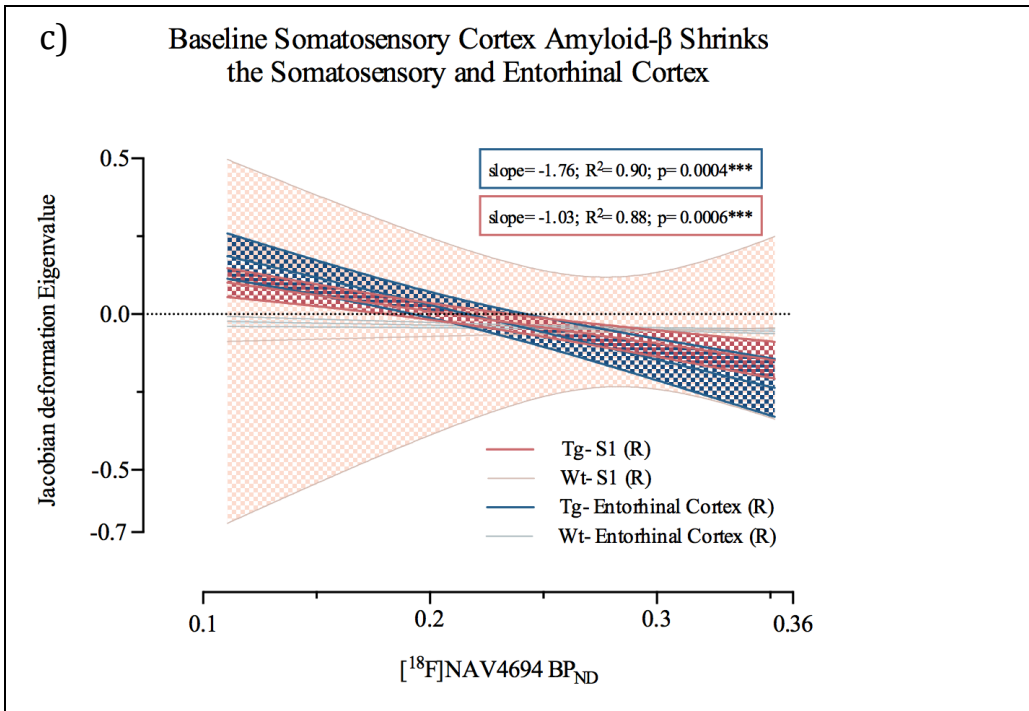


Figure 5. *t*-statistical maps showing regions of significant correlation between somatosensory cortex NAV seed with longitudinal DBM. The areas correspond to a) right primary somatosensory cortex and b) right entorhinal cortex. c) Graphical representation of somatosensory cortex NAV correlation with longitudinal deformation changes.

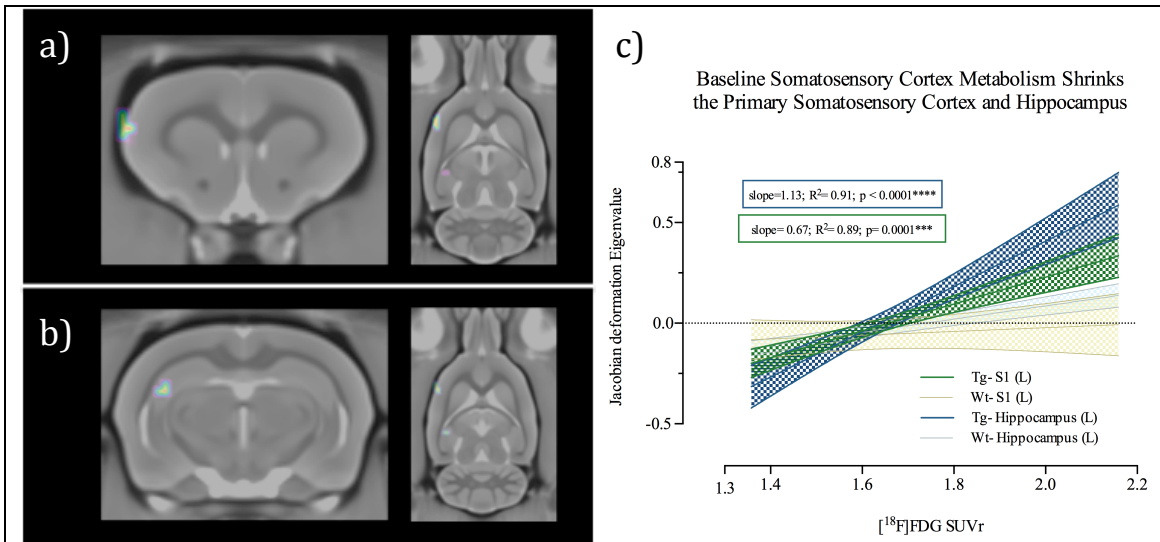
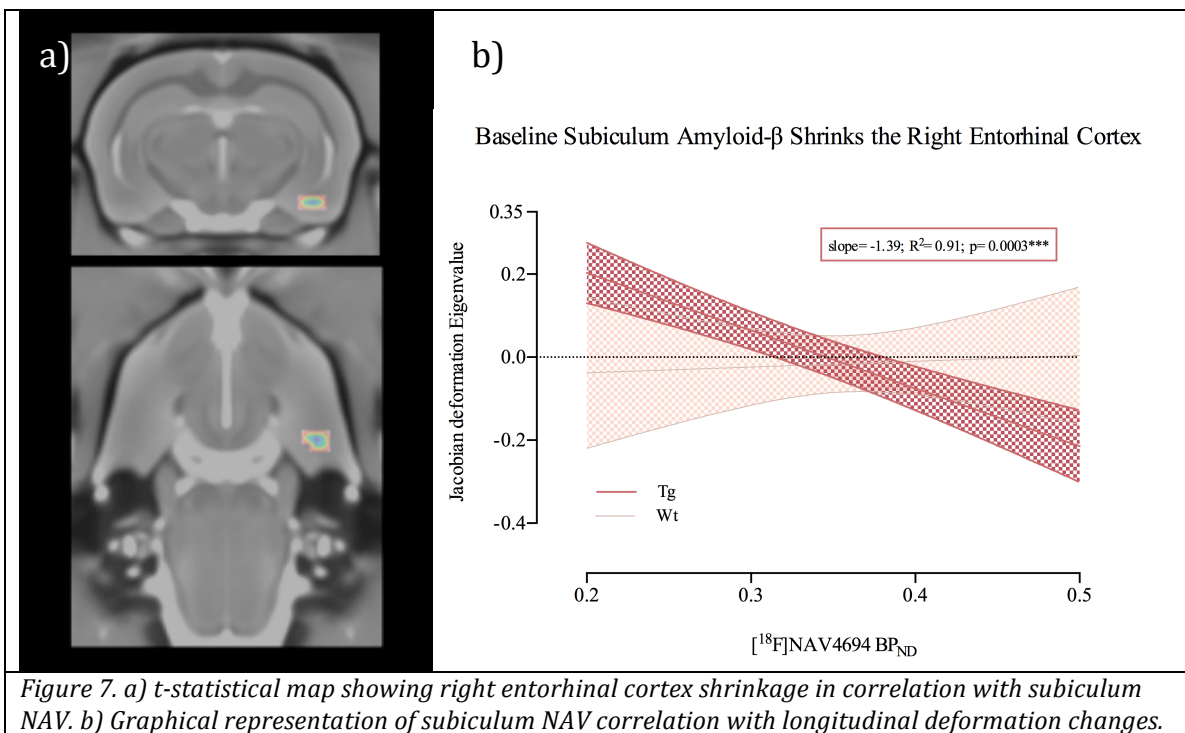
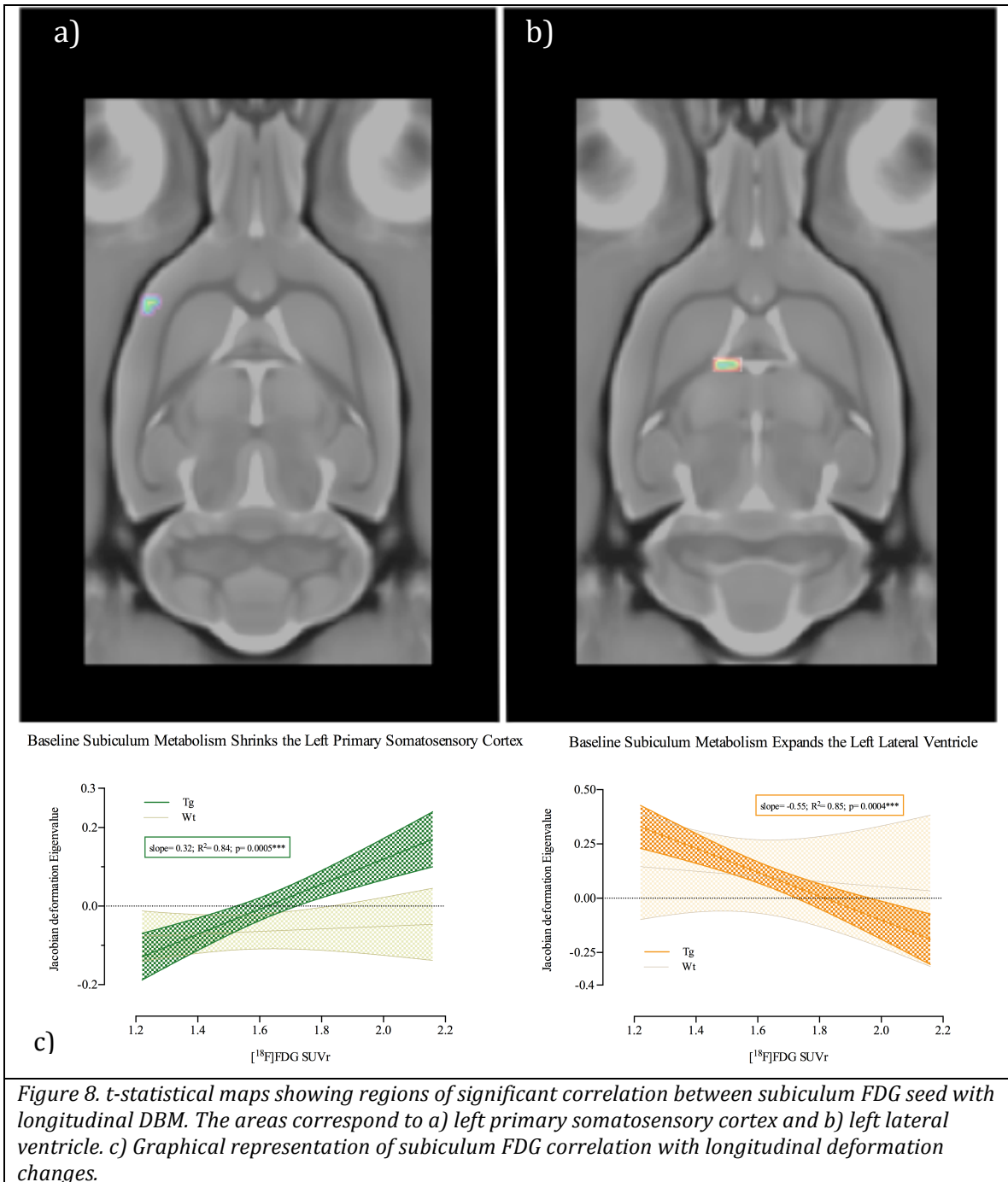


Figure 6. *t*-statistical maps showing regions of significant correlation between somatosensory cortex FDG seed with longitudinal DBM. The areas correspond to a) left primary somatosensory cortex and b) left hippocampus. c) Graphical representation of somatosensory cortex FDG correlation with longitudinal deformation changes.

## Subiculum

Again, resembling the correlations seen with the hippocampal and the somatosensory amyloidosis, the subiculum amyloidosis revealed a negative correlation with the right entorhinal cortex (slope coefficient= -1.39,  $R^2= 0.91$ ,  $p=0.0003^{***}$ ) (Figure 7). Moreover, an overlapping finding to hippocampal hypometabolism appeared when correlating subiculum hypometabolism with DBM, which is a positive correlation with the left primary somatosensory cortex (slope coefficient= 0.32,  $R^2= 0.84$ ,  $p=0.0005^{***}$ ) and a negative correlation with the left lateral ventricle (slope coefficient= -0.55,  $R^2= 0.85$ ,  $p=0.0004^{***}$ ) (Figure 8).





## Discussion

### *Amyloidosis and Atrophy*

Our findings of region-specific longitudinal neurodegeneration of McGill-R-Thy1-APP Tg rats in correlation with baseline levels of amyloid support the notion that

there exists a spatial pattern of atrophy in brains expressing high loads of amyloid plaque. Specifically, amyloidosis in the frontal cortex correlated with the atrophy of the left secondary and the right primary somatosensory cortices. To emphasize, the right entorhinal cortex degeneration correlated with the amyloid load in all seed ROIs except for the frontal cortex. This eminent presence of atrophy, in correlation with amyloid load, confirmed the vulnerability of the entorhinal cortex in AD (18; 19) and stresses its crucial role. Gateway functions of the entorhinal cortex, such as, connecting the neocortex and the hippocampus formation (20), receiving afferents from the association and limbic areas, projecting to the hippocampus, receiving afferents from the hippocampus, and sending afferents back to the association cortices (21), may attribute to the this volumetric finding specific to AD.

The mechanism of degeneration is still an area of research that questions whether the reducing of entorhinal cortex volume is due to either neuronal or synaptic loss. However, our significant regional finding supports previous studies in humans showing that the amount of neuronal loss in the entorhinal cortex of AD brains parallels neuritic changes including plaques (22). The specificity of the entorhinal cortex as a vulnerable hallmark of AD has been confirmed by the absence of substantial neuronal loss of this region in healthy aging (20).

To summarize, the relationship between the rate of brain atrophy and the whole brain and regional amyloidosis in humans has been found to be positive (23), and our data supports this finding, with the absence of any positive correlation. These results further confirm that the central role of amyloid lies in the pathogenesis of AD and that McGill-R-Thy1-APP Tg rat model is adequate for translational studies. Our model of approach implies interdependent roles for MRI and NAV imaging in AD.

### *Hypometabolism and Atrophy*

Several studies have indicated functional disruption as a contributing mechanism to distant atrophy pattern of AD (24). Here, we also observed atrophy of distant

regions caused by early hypometabolism in specific brain areas, analyzed by correlative studies of baseline FDG-PET and longitudinal DBM. Both the hippocampus and the subiculum hypometabolism correlated well with the shrinkage of the left primary somatosensory cortex and the expansion of the left lateral ventricle, with the addition of the expansion the fimbria of the left hippocampus in case of hippocampal hypometabolism. While the right entorhinal cortex was specified as the degeneratively vulnerable region that correlated the best with amyloidosis, in the case of hypometabolism, the left primary somatosensory cortex stood out in accordance with decreased metabolism in all areas except for the frontal cortex. The frontal cortex hypometabolism revealed a unique region, which is the left insular cortex. The decreased metabolism of the somatosensory cortex showed correlation with the left hippocampus as well.

All the regional significances found in our study support a previous study showing an overlap of hypometabolism and atrophy in the hippocampal regions, temporal neocortex, insula and middle and orbital frontal areas, suggesting the existence of a causal relationship between the level of metabolism with atrophy pattern (24). The expansion of the lateral ventricle was apprehended, since it is a well-known fact that ventricle expansion clinically accompanies AD progression (25), with probable representation for global atrophy occurring in the brain.

Atrophy of the insula also mirrors previous studies focusing on grey matter atrophy in AD patients, which have detected unexpected decrease of not only the insula but also the caudate nucleus (24, 26). A possible explanation of insular atrophy comes from its abundant connections with the temporal pole and the superior temporal sulcus of the temporal lobe, along with local intra-insular connections. The presence of these connections and projects to subdivisions of the cingulate gyrus, amygdaloidal and non-amygdaloidal connections such as perirhinal, entorhinal and periamygdaloid cortices, have confirmed the role of insula as a limbic integration cortex. In addition, its role as a somatosensory area, multifaceted sensory area and involvement in AD explains the atrophy seen in the left somatosensory cortex (27).

Although our analysis did not include hypometabolism hallmark regions of human AD patients, future studies involving those, such as the parieto-temporal, posterior cingulate-precuneous area, and the anterior cingulate cortex (28) should be designed to reveal relationships between these regional hypometabolisms and atrophy patterns. Since the hypometabolism of the posterior association cortex, especially the posterior cingulate cortex, is a region that shows dramatic decrease in metabolism in AD, whether this indicates a distant effect of neuronal damage in the hippocampus, via the cingulum bundle, needs further investigation (29).

### *Advantage of Our Analytic Method*

Analysis of in-vivo images illustrating causative relationship patterns of amyloid deposition, hypometabolism and neurodegeneration contribute as an insight about affected brain networks and can help identify vulnerable regions for use as biomarkers of AD. Fastly emerging therapeutic approaches in attempt to modify AD stresses the importance of early diagnosis and disease monitoring (30). In addition, the use of automated voxel-level DBM fulfills the need of techniques that accurately localize atrophy in an unbiased manner, providing means of modeling changes over the whole brain without the problem of operator-dependent inter-subject variability, eliminating the restriction that imposes a priori judgment (26).

Since many cognitively normal individuals show high prevalence of A $\beta$  positivity (31, 32), even though they are one of the major defining pathological features of AD, diagnosis solely on amyloid PET itself brings about potential error in case-selection procedure. Instead of focusing on a single imaging modality, using a combination of methods provides a helpful guide to avoid this risk. Therefore, age-related amyloid detection, along with cross-examination of other AD-related biomarkers, may prevent the occurrence of such misinterpretations with unsuspected early AD cases (32). Integration of AD pathological hallmarks aid in providing a helpful insight to

track disease progression, which can be applicable in clinical trials of new therapies that target specific biomarkers at different stages of the disease (30).

An advantage that comes with the utilization of Tg rats displaying familial genetic case of AD is that the young age of onset minimizes confounding effect of age-related comorbidity. Not only is age a problematic issue when studying diseases of the elderly population, but also, a wide range of psychiatric problems, due to the increase in prevalence of mixed-cause dementia with age, introduces complexity when examining AD patients. Moreover, rats representing similar amyloidogenic progression as humans aid in overcoming the difficulty associated with translation of research findings to clinical populations (32).

### *Limitations/Improvements*

The most evident weakness of our study comes from the limited number of rats that were utilized. Despite our effort to initiate this longitudinal study with a cohort of enough statistical power, the 15 WT and 15 Tg rats faced physical complications, leading to the reduction of our sample size to between 4 and 9 rats per group. Additionally, the acquisition of imaging data from only 2 time points does not fully illustrate the complete clinical progression of AD. By the follow-up time point, the rats were only 19 months old, which is approximately the age of 40 in humans (33). Also, age-to-age comparison may not be the best interpretation when studying the Tg rats, since while AD is a progressive neurodegenerative disease that spans for more than 20 years with age of onset before 65 (34), the rats develop plaque deposition as early as 6 months (8, 13), which is about age of 10 in humans. Looking into two time points does not provide information that is representative enough to map out the full biomarker changes occurring in the McGill-R-Thy1-APP rats, and a technique for solving the differences in aging processes of animals and humans is necessary for successful translational studies.

Voxel-level DBM approach provides an unbiased method for assessing volumetric changes over the whole brain. However, deviation in the shape or anatomical position of a particular structure may be a weakness of this technique, especially when focusing on smaller regions that have large surface area-to-volume ratio (30). Another limitation of our study comes from the presence of variable plaque loads among the Tg rats used (R), which indicates that the onset of spreading of amyloid pathology fluctuates according to individual differences.

### *Future Directions*

Successful translational studies using our animal results of complementary imaging modalities with human studies for prediction of future cognitive course in patients with AD. Incorporating more time points from both earlier and later stages can aid in revealing of alterations of significant sites of atrophy as the disease advances.

Our analysis used the DBM to correlate with baseline levels of amyloidosis and metabolism, but interchanging the dependent and independent variables to correlate baseline amyloidosis with progressive hypometabolism in different regions, would also provide a useful insight for spatio-temporal changes in AD, as it is already known that decrease in metabolism occurs following amyloid deposition (3).

Focusing on the areas that are discovered to show atrophy in our study, a more in-depth analysis at cellular level to identify whether this decline is at the level of synapses or is actual neuronal loss, is required. In order to improve the statistical power, a larger and longitudinally followed cohort with a more complete and consistently accumulated data on imaging and fluid biomarker, is needed. Eventual success of full validation of biomarker pathologies of the rat model of AD may aid in even earlier clinical evaluation of risk for AD, developing methods for stratifying those with likelihood of facing cognitive decline (9).

### *Conclusion*

Overall, our preliminary data showing that amyloidosis and hypometabolism pertain to different regional atrophy, validates findings that, in AD, the

neuropathology follows a gradual, stereotypical progression through phases that are defined for A $\beta$  deposition (36). The presence of relationships between baseline levels of amyloidosis and hypometabolism with atrophy pattern only in the Tg, not the WT rats, is consistent with the hypothesis that the process of AD and aging do not belong as a part of a continuous aging spectrum, but rather as dichotomous processes. The differences in locations of atrophy depending on the biomarker expression explain the intrinsic variability in susceptibilities to discrete pathological expressions in AD. Although the expected AD hallmark areas were detected, including the hippocampus and the entorhinal cortex, the absence of other hallmark cortical regions suggest that the complete neurodegeneration profile not only results from A $\beta$  alone, but is likely to be from the synergistic effect of A $\beta$  and tau (35, 37, 38).

Incorporation of advancing neuroimaging techniques, which allow accurate measurement of atrophy, metabolism, inflammation, amyloid plaques, and NFT load, along with fluid biomarkers, will bring about the possibility for preclinical detection of AD, as promising tools for early diagnosis and disease monitoring (9). Different diagnostic methods serve as valuable assessment approaches in testing the efficacy of region-specific disease-modifying treatments.

## Bibliography

1. Nilsen, Linn H., Torun M. Melø, Oddbjørn Sæther, Menno P. Witter, and Ursula Sonnewald. "Altered neurochemical profile in the McGill-R-Thy1-APP rat model of Alzheimer's disease: a longitudinal in vivo 1H MRS study." *Journal of neurochemistry* 123, no. 4 (2012): 532-541.
2. Terry, Robert D., Eliezer Masliah, David P. Salmon, Nelson Butters, Richard DeTeresa, Robert Hill, Lawrence A. Hansen, and Robert Katzman. "Physical basis of cognitive alterations in Alzheimer's disease: synapse loss is the major correlate of cognitive impairment." *Annals of neurology* 30, no. 4 (1991): 572-580.
3. Jack, Clifford R., David S. Knopman, William J. Jagust, Ronald C. Petersen, Michael W. Weiner, Paul S. Aisen, Leslie M. Shaw et al. "Tracking

- pathophysiological processes in Alzheimer's disease: an updated hypothetical model of dynamic biomarkers." *The Lancet Neurology* 12, no. 2 (2013): 207-216.
4. Hardy, John A., and Gerald A. Higgins. "Alzheimer's disease: the amyloid cascade hypothesis." *Science* (1992).
  5. Gallagher, Michela, and Peter R. Rapp. "The use of animal models to study the effects of aging on cognition." *Annual review of psychology* 48, no. 1 (1997): 339-370.
  6. Maheswaran, Satheesh, Hervé Barjat, Daniel Rueckert, Simon T. Bate, David R. Howlett, Lorna Tilling, Sean C. Smart et al. "Longitudinal regional brain volume changes quantified in normal aging and Alzheimer's APP× PS1 mice using MRI." *Brain research* 1270 (2009): 19-32.
  7. Tesson, Laurent, Jean Cozzi, Severine Menoret, Severine Remy, Claire Usal, Alexandre Fraichard, and Ignacio Anegon. "Transgenic modifications of the rat genome." *Transgenic research* 14, no. 5 (2005): 531-546.
  8. Leon, Wanda Carolina, Fabio Canneva, Vanessa Partridge, Simon Allard, Maria Teresa Ferretti, Arald DeWilde, Freya Vercauteren et al. "A Novel Transgenic Rat Model with a Full Alzheimer's-Like Amyloid Pathology Displays Pre-Plaque Intracellular Amyloid- $\beta$ -Associated Cognitive Impairment." *Journal of Alzheimer's Disease* 20, no. 1 (2010): 113-126.
  9. Perrin, Richard J., Anne M. Fagan, and David M. Holtzman. "Multimodal techniques for diagnosis and prognosis of Alzheimer's disease." *Nature* 461, no. 7266 (2009): 916-922.
  10. Jack, Clifford R., Val J. Lowe, Matthew L. Senjem, Stephen D. Weigand, Bradley J. Kemp, Maria M. Shiung, David S. Knopman et al. "<sup>11</sup>C PiB and structural MRI provide complementary information in imaging of Alzheimer's disease and amnesic mild cognitive impairment." *Brain* 131, no. 3 (2008): 665-680.
  11. Chételat, G., B. Desgranges, B. Landeau, F. Mézenge, J. B. Poline, V. De La Sayette, F. Viader, F. Eustache, and J-C. Baron. "Direct voxel-based comparison between grey matter hypometabolism and atrophy in Alzheimer's disease." *Brain* 131, no. 1 (2008): 60-71.
  12. Tustison, Nicholas J., Brian B. Avants, Philip Cook, Yuanjie Zheng, Alexander Egan, Paul Yushkevich, and James C. Gee. "N4ITK: improved N3 bias correction." *Medical Imaging, IEEE Transactions on* 29, no. 6 (2010): 1310-1320.

13. Heggland, Ingrid, Inge S. Storakaas, Hanne T. Soligard, Asgeir Kobro-Flatmoen, and Menno P. Witter. "Stereological estimation of neuron number and plaque load in the hippocampal region of a transgenic rat model of Alzheimer's disease." *European Journal of Neuroscience* 41, no. 9 (2015): 1245-1262.
14. Chung, M. K., K. J. Worsley, T. Paus, C. Cherif, D. L. Collins, J. N. Giedd, J. L. Rapoport, and A. C. Evans. "A unified statistical approach to deformation-based morphometry." *NeuroImage* 14, no. 3 (2001): 595-606.
15. Rowe, Christopher C., and Victor L. Villemagne. "Brain amyloid imaging." *Journal of nuclear medicine technology* 41, no. 1 (2013): 11-18.
16. Gunn, Roger N., Adriaan A. Lammertsma, Susan P. Hume, and Vincent J. Cunningham. "Parametric imaging of ligand-receptor binding in PET using a simplified reference region model." *Neuroimage* 6, no. 4 (1997): 279-287.
17. Paxinos, G., and C. Watson. "The Rat Brain in Stereotaxic Coordinates. 6th edn Elsevier: Amsterdam." (2006).
18. Hyman, Bradley T., Gary W. Van Hoesen, Antonio R. Damasio, and Clifford L. Barnes. "Alzheimer's disease: cell-specific pathology isolates the hippocampal formation." *Science* 225, no. 4667 (1984): 1168-1170.
19. Braak, H., and E. Braak. "Neuropathological staging of Alzheimer-related changes." *Acta neuropathologica* 82, no. 4 (1991): 239-259.
20. Gómez-Isla, Teresa, Joseph L. Price, Daniel W. McKeel Jr, John C. Morris, John H. Growdon, and Bradley T. Hyman. "Profound loss of layer II entorhinal cortex neurons occurs in very mild Alzheimer's disease." *The Journal of neuroscience* 16, no. 14 (1996): 4491-4500.
21. Zola-Morgan, Stuart, Larry R. Squire, and Seth J. Ramus. "Severity of memory impairment in monkeys as a function of locus and extent of damage within the medial temporal lobe memory system." *Hippocampus* 4, no. 4 (1994): 483-495.
22. West, Mark J., Paul D. Coleman, Dorothy G. Flood, and Juan C. Troncoso. "Differences in the pattern of hippocampal neuronal loss in normal ageing and Alzheimer's disease." *The Lancet* 344, no. 8925 (1994): 769-772.
23. Archer, Hilary A., Paul Edison, David J. Brooks, Jo Barnes, Chris Frost, Tom Yeatman, Nick C. Fox, and Martin N. Rossor. "Amyloid load and cerebral atrophy in Alzheimer's disease: An 11C-PIB positron emission tomography study." *Annals of neurology* 60, no. 1 (2006): 145-147.

24. Chételat, G., B. Desgranges, B. Landeau, F. Mézenge, J. B. Poline, V. De La Sayette, F. Viader, F. Eustache, and J-C. Baron. "Direct voxel-based comparison between grey matter hypometabolism and atrophy in Alzheimer's disease." *Brain* 131, no. 1 (2008): 60-71.
25. Haxby, J. V., J. A. Gillette, D. Teichberg, S. I. Rapoport, and M. B. Schapiro. "Longitudinal changes in lateral ventricular volume in patients with dementia of the alzheimer type." *Neurology* 42, no. 10 (1992): 2029-2029.
26. Rombouts, Serge ARB, Frederik Barkhof, Menno P. Witter, and Philip Scheltens. "Unbiased whole-brain analysis of gray matter loss in Alzheimer's disease." *Neuroscience letters* 285, no. 3 (2000): 231-233.
27. Augustine, James R. "Circuitry and functional aspects of the insular lobe in primates including humans." *Brain Research Reviews* 22, no. 3 (1996): 229-244.
28. Mosconi, Lisa. "Brain glucose metabolism in the early and specific diagnosis of Alzheimer's disease." *European journal of nuclear medicine and molecular imaging* 32, no. 4 (2005): 486-510.
29. Villain, Nicolas, Béatrice Desgranges, Fausto Viader, Vincent De La Sayette, Florence Mézenge, Brigitte Landeau, Jean-Claude Baron, Francis Eustache, and Gaël Chételat. "Relationships between hippocampal atrophy, white matter disruption, and gray matter hypometabolism in Alzheimer's disease." *The Journal of neuroscience* 28, no. 24 (2008): 6174-6181.
30. Scahill, Rachael I., Jonathan M. Schott, John M. Stevens, Martin N. Rossor, and Nick C. Fox. "Mapping the evolution of regional atrophy in Alzheimer's disease: unbiased analysis of fluid-registered serial MRI." *Proceedings of the National Academy of Sciences* 99, no. 7 (2002): 4703-4707.
31. Crystal, Hi, D. Dickson, P. Fuld, D. Masur, R. Scott, M. Mehler, J. Masdeu, C. Kawas, M. Aronson, and L. Wolfson. "Clinico-pathologic studies in dementia Nondemented subjects with pathologically confirmed Alzheimer's disease." *Neurology* 38, no. 11 (1988): 1682-1682.
32. Johnson, Keith A., Satoshi Minoshima, Nicolaas I. Bohnen, Kevin J. Donohoe, Norman L. Foster, Peter Herscovitch, Jason H. Karlawish et al. "Appropriate use criteria for amyloid PET: a report of the Amyloid Imaging Task Force, the Society of Nuclear Medicine and Molecular Imaging, and the Alzheimer's Association." *Journal of Nuclear Medicine* 54, no. 3 (2013): 476-490.
33. Quinn, Robert. "Comparing rat's to human's age: how old is my rat in people years?." *Nutrition* 21, no. 6 (2005): 775-777.

34. Goate, Alison, Marie-Christine Chartier-Harlin, Mike Mullan, Jeremy Brown, Fiona Crawford, Liana Fidani, Luis Giuffra et al. "Segregation of a missense mutation in the amyloid precursor protein gene with familial Alzheimer's disease." *Nature* 349, no. 6311 (1991): 704-706.
35. Heggland, Ingrid, Inge S. Storakaas, Hanne T. Soligard, Asgeir Kibro-Flatmoen, and Menno P. Witter. "Stereological estimation of neuron number and plaque load in the hippocampal region of a transgenic rat model of Alzheimer's disease." *European Journal of Neuroscience* 41, no. 9 (2015): 1245-1262.
36. Thal, Dietmar R., Udo Rüb, Mario Orantes, and Heiko Braak. "Phases of A $\beta$ -deposition in the human brain and its relevance for the development of AD." *Neurology* 58, no. 12 (2002): 1791-1800.
37. Knopman, David S., Clifford R. Jack, Heather J. Wiste, Stephen D. Weigand, Prashanthi Vemuri, Val J. Lowe, Kejal Kantarci et al. "Selective worsening of brain injury biomarker abnormalities in cognitively normal elderly persons with  $\beta$ -amyloidosis." *JAMA neurology* 70, no. 8 (2013): 1030-1038.
38. Wang, Liang, Tammie L. Benzinger, Jason Hassenstab, Tyler Blazey, Christopher Owen, Jingxia Liu, Anne M. Fagan, John C. Morris, and Beau M. Ances. "Spatially distinct atrophy is linked to  $\beta$ -amyloid and tau in preclinical Alzheimer disease." *Neurology* 84, no. 12 (2015): 1254-1260.

# Hippocampal Volumetry Analysis

## Materials and Methods

All experimental procedures involved in this study were approved by the McGill Animal Care ethics committee and were carried out following the Canadian Council on Animal Care guidelines. The animals were provided by Dr. A. Claudio Cuello at the department of pharmacology at McGill University in Montreal, Quebec, Canada. Housing for the rats were held at the animal facility of the Douglas Mental Health University Institute with a 12/12h light/darkness cycles.

### *Total Cohort*

We began with 12 medically healthy wild-type (Wt) Wistar rats and 13 medically healthy homozygous McGill-Thy1-R-APP transgenic (Tg) rats. At baseline, the average weights of the 6 male and 6 female Wt rats were  $639.17 \pm 37.39$  g and  $361.67 \pm 28.81$  g, respectively. Similarly, the 7 male and 6 female Tg rats weighed in at  $613.00 \pm 55.92$  g and  $353.17 \pm 14.19$  g.

### *Longitudinal Cohort*

All 12 Wt and 13 Tg rats were successfully scanned for baseline acquisition of MRI and PET at 9-11 months after birth. By the time for the 16-19 month follow-up MRI and PET measures, the numbers had reduced to 5 Wt (2 males, 3 females) and 9 Tg (3 males, 6 females) rats. The loss of cohort was due to a variety of complications including tumours of the brain, abdomen and legs, pneumonia and unknown causes. The weights the longitudinal cohort were, on average,  $603.00 \pm 4.24$  g for male and  $359.33 \pm 26.27$  g for female Wt rats. The average weights for the male and female Tg rats were  $578.33 \pm 58.18$  g and  $353.17 \pm 14.19$  g, respectively at baseline.

At follow-up, the average weights were  $660.00 \pm 8.49$  g and  $425.00 \pm 61.83$  g for the male and the female WT rats, while the Tg male and female rats weighted in at  $650.33 \pm 76.43$  g and  $408.00 \pm 21.27$  g each.

## *Manual Hippocampal Segmentation*

Hippocampal 3D manual volumetry was performed using the image analysis software Display, which allows the user to manually select the region of interest (ROI) for volumetric calculation of that region. The hippocampal formation was manually segmented to include the dentate gyrus, the hippocampus proper, and the subiculum. The sagittal view of the MRI was used for preliminary manual segmentation. Adjustments were guided by the correspondent lateral and coronal views of the brains.

### **Lateral to Medial (Sagittal View)**

The first step of hippocampal segmentation was carried out on the sagittal view of the rat brain. Starting from the very lateral edge of the brain, the 3D image was carefully scrolled, slice-by-slice, towards the medial portion. Due to the natural position of the hippocampus in the rat brain, the segmentation was carried out from the temporal (caudo-ventral) towards the septal (rostro-dorsal) hippocampal areas.

After the appearance of the outermost cortical regions consisting of primary and secondary auditory cortex, the disappearance of deep cerebral white matter and the lateral ventricle demarcated the initiation point of hippocampal segmentation (Figure 1).

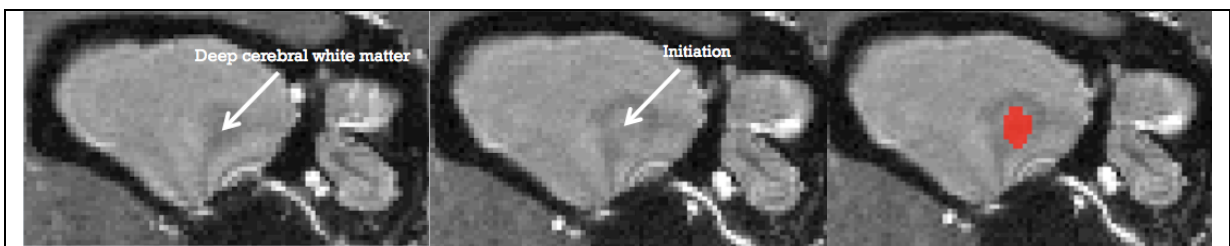
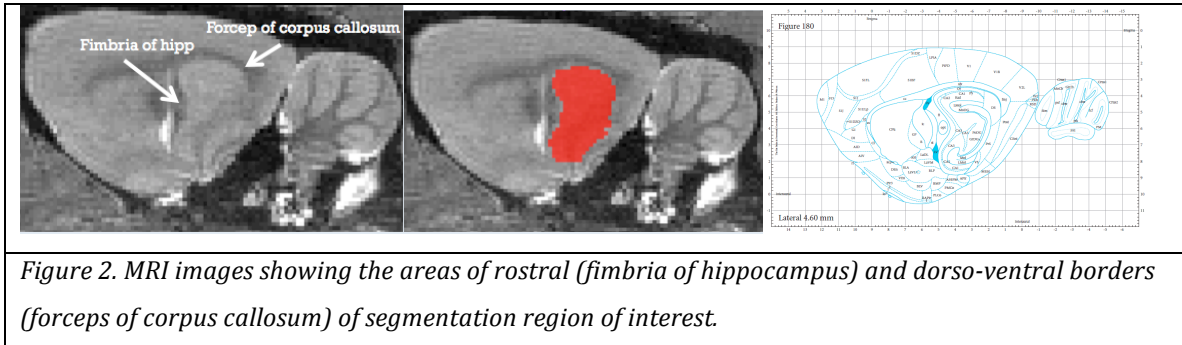
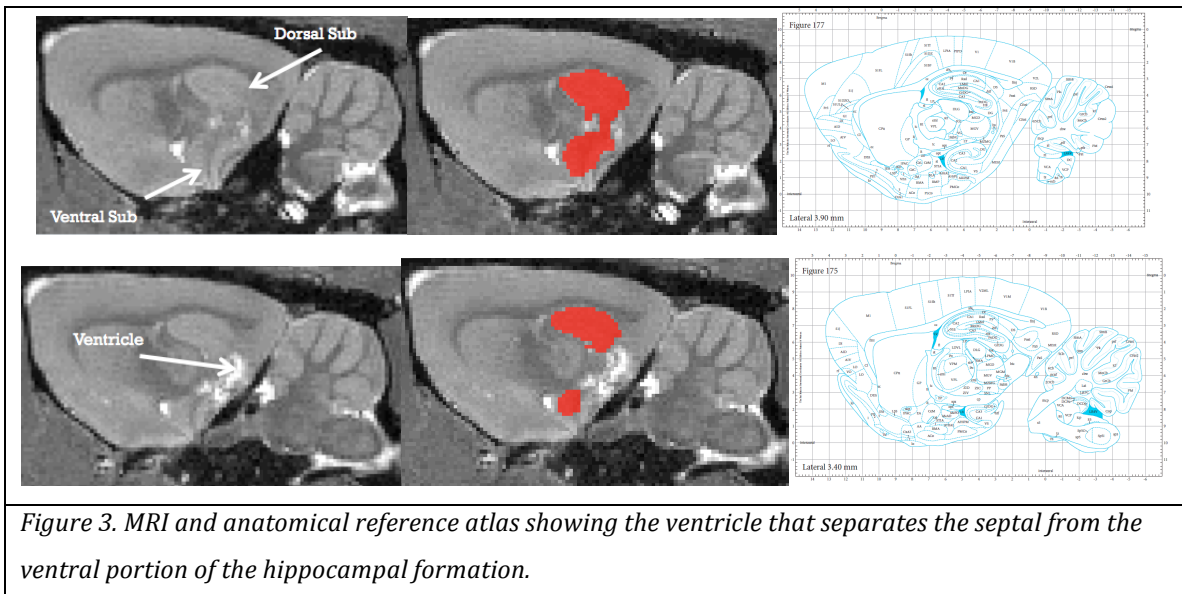


*Figure 1. Lateral towards medial slice-by-slice of MRI image (left to right) to demonstrate the Initiation point of hippocampus segmentation.*

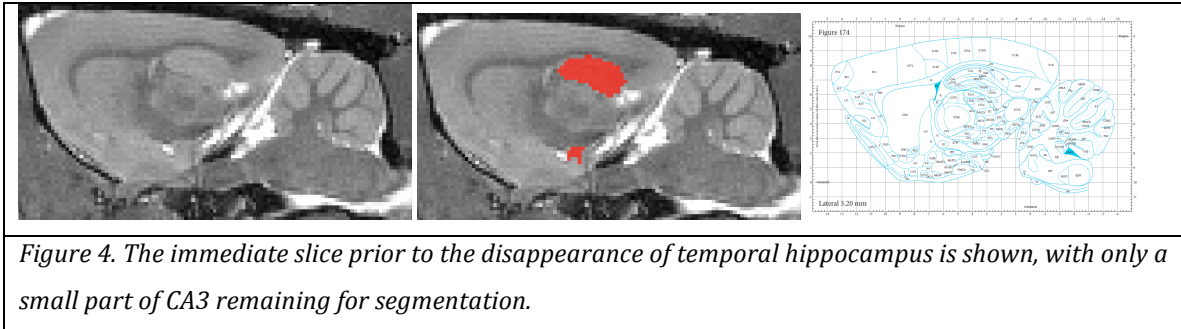
The layers of the CA1 region located in the intermediate portion (in the septo-temporal axis perspective) of the hippocampal formation appeared in the order of: stratum oriens, pyramidal cell layer, and stratum radiatum. The strong white fimbria of the hippocampus set the rostral border while deep cerebral white matter and fibers of the corpus callosum set the dorso-ventral border (Figure 2).



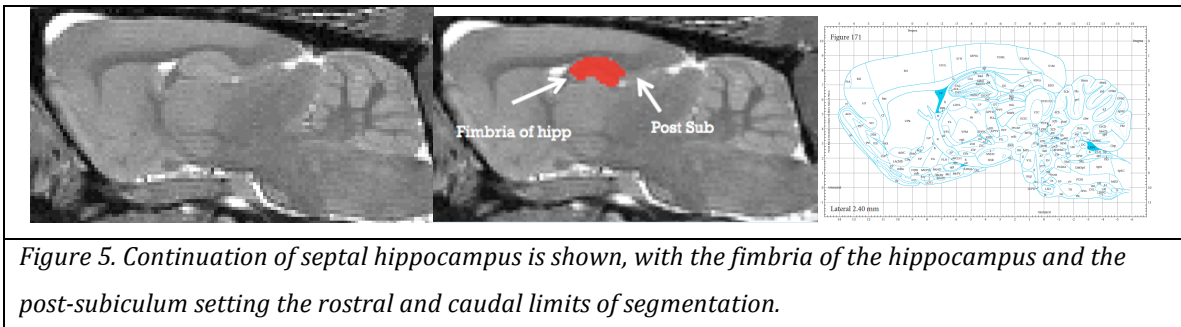
Eventually, the segmentation process migrated deeper until rostrally located CA3 and caudally located subiculum disappeared from center portion of the hippocampus, followed by the dentate gyrus. As the segmentation progressed medially, the lateral ventricle and white matter separated the septal from the temporal portions. Along with the CA fields and the dentate gyrus, the septal segmentation included the dorsal subiculum while the temporal portion consisted the ventral subiculum (Figure 3).



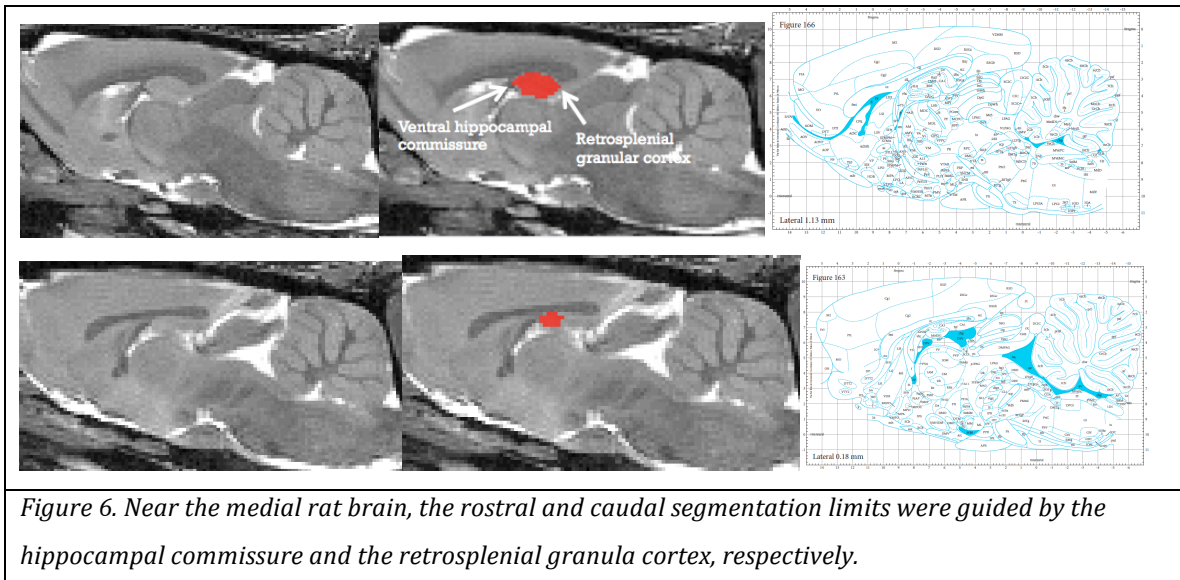
Segmentation of the temporal portion of the hippocampus terminated prior to the septal region due to its gradual disappearance as the process progressed towards the medial view. CA3 was the last region to remain until the termination of temporal hippocampus segmentation (Figure 4).



The segmentation of dorsal (septal) portion of the hippocampus continuously consisted of the CA fields, the DG and the dorsal subiculum. The fimbria of the hippocampus served as the rostral anterior border while the post-subiculum guided the caudal posterior limit (Figure 5).



As the medial limit approached, segmentation was guided by the retrosplenial granular cortex at posterior border and by the ventral hippocampal commissure at the anterior limit. The dorsal hippocampal commissure also demonstrated to serve good contrast for easy identification of the hippocampus (Figure 6).



After completion of one hemisphere, the opposite hemisphere was segmented using the identical guidelines, from lateral towards the medial section of the brain.

### **Dorsal to Ventral (Lateral view)**

Due to the position of the hippocampal formation in the rat brain, going from the dorsal towards ventral direction led to septal towards temporal parts of the hippocampus. After passing through the cortical layers of the medial parietal association cortex, followed by the corpus callosum, the segmentation began with the appearance of the DG, surrounded by the CA regions present in the septal hippocampus. Deep cerebral white matter made clear dark borders around the hippocampus. As the process is carried down towards the ventral (temporal) portion of the hippocampus, the fimbria of the hippocampus and the lateral ventricle set the lateral borders.

There is no visibly concrete landmark that demarcates the posterior limit around the intermediate portion of the septotemporal axis of the hippocampus; therefore, the segmentor carefully selected the subicular complexes while exempting the entorhinal cortex. The medial region of the hippocampus was carefully selected so that the ventral medial geniculate nucleus, which is present medially to the DG, was not included. As the segmentation progressed deeper

towards the ventral section of the brain, the cerebral peduncle replaced the ventral medial geniculate nucleus as the medial border of the hippocampus. Manual segmentation proceeded, mainly guided by the deep cerebral white matter as the rostro-ventral borders, until the disappearance of CA3, followed by the ventral subiculum.

### **Anterior to Posterior/Rostral to Caudal (Coronal view)**

Going from anterior to posterior portion of the brain, segmentation initiated when CA3, surrounded by the oriens layer, started to appear, which represents the septal end of the hippocampal formation. The surrounding fimbria set the borders that distinguished the region of interest. Segmentation continued as radiatum layer, stratum lucidum and the DG also appeared to be selected. The dorsal and ventral borders were set by the dorsal hippocampal commissure as well as the laterodorsal thalamic nuclei and the stria medullaris thalamus, respectively.

As the segmentation progressed towards the posterior brain, the temporal end of the hippocampal formation, which consisted of the oriens layer of CA3, started to appear. Stratum lucidum and radiatum layers were the following regions of interest to be manually selected, quickly followed by the rest of the CA regions. At this point, the lateral ventricle and the thalamus marked the lateral and medial limits, while the amygdala set the ventral border. Dorsal subiculum at the top end of the hippocampus and ventral subiculum at the bottom end were carefully selected to be included as our region of interest. Eventually, segmentation terminated with the disappearance of CA1 layers and DG, followed by the subiculum at the intermediate section of the septo-temporal axis.

### ***Intracranial Volume Manual Segmentation***

The intracranial regions were traced to measure the intracranial (IC) volume, which included the grey and the white matter without the ventricles. The calculated volumes were used to normalize the raw hippocampal volumes, resulting in

normalized hippocampal volumes, which would account for variables such as differences in head and brain sizes of the rats.

### *Statistical Analysis*

Normalized hippocampal volumes were compared using mixed model 2-way ANOVA, with age and group as the within and between group factors, respectively. For validation of our method, intra-rater stability was calculated using SPSS (Intra-Class Correlation).

## Results

### *Cohort*

Initially, 16 Wild-type and 15 transgenic littermates were assigned for the use of this study. Due to the years that took to follow up on these rats, there were significant health issues that the animals faced. As a result, only 5 wild-type and 9 transgenic rats, for a total of 14, were included in the longitudinal volumetric analysis. As for the correlation analyses, 4 wild-type and 8 transgenic rats survived for NAV, and 5 wild-type and 9 transgenic rats survived for FDG.

### *Volumetric Analysis*

#### **Raw Hippocampal Volume:**

The two groups of animals' hippocampal volumes did not differ at baseline; the average for the Wt and tg groups were  $79.0000 \pm 8.1706 \text{ mm}^3$  and  $78.2450 \pm 5.8221 \text{ mm}^3$ , respectively. By the time for follow-up analysis, the average volumes measured at  $80.4300 \pm 5.1744 \text{ mm}^3$  and  $74.6067 \pm 6.6295 \text{ mm}^3$  for Wt and Tg, respectively, showing 7.24% of group differences (Table 1, Figure 7-A).

**Table 1. 2-way ANOVA statistical analysis of raw hippocampal values showed significance in the interaction of time and group factors at  $F(1,12) = 7.774$  ( $p = 0.0164^*$ ).**

Wild-Type	Transgenic	Difference
-----------	------------	------------

Baseline	79.00±8.17 mm <sup>3</sup>	78.2450±5.82 mm <sup>3</sup>	<b>0.96%</b>
Follow-up	80.43±5.17 mm <sup>3</sup>	74.6067±6.63 mm <sup>3</sup>	<b>7.24%*</b>
<b>Difference</b>	<b>-1.81%</b>	<b>4.65% *</b>	

### Intracranial Volume:

The average intracranial volumes of Wt rats were 2191.6201±110.5623 mm<sup>3</sup> and 2268.6433±116.2682 mm<sup>3</sup> at baseline and follow-up, respectively. As for the Tg rats, the baseline and follow-up average intracranial volumes were 2092.4241±121.4420 mm<sup>3</sup> and 2166.2721±123.2318 mm<sup>3</sup> (Table 2, Figure 7-B).

**Table 2. 2-way ANOVA statistical analysis of the intracranial volumes showed only significant age effect at F(1,12)=108.0 (p<0.0001\*\*\*\*)**

	<b>Wild-Type</b>	<b>Transgenic</b>	<b>Difference (Wt&gt;Tg)</b>
Baseline	2191.62±110.56 mm <sup>3</sup>	2092.42±121.44 mm <sup>3</sup>	<b>4.53%</b>
Follow-up	2268.64±116.27 mm <sup>3</sup>	2166.27±123.23 mm <sup>3</sup>	<b>4.51%</b>
<b>Difference</b>	<b>3.51%****</b>	<b>3.53%****</b>	

**(FU>BS)**

### Normalized Hippocampal Volume:

The normalization procedure was completed simply by taking the raw hippocampal volume and dividing by the intracranial volume for each animal. As a result, this step yielded a ratio representing the amount of brain volume the hippocampus took part of, taking into account the size differences between individual rats (Table 3, Figure 7-C).

**Table 3. 2-way ANOVA statistical analysis of normalized hippocampus volumes showed significant interaction factor at F(1,12)= 7.841 (p=0.016\*)**

	<b>Wild-Type</b>	<b>Transgenic</b>	<b>Difference (Wt&gt;tg)</b>
Baseline	0.0360±0.0020	0.0374±0.0015	<b>-3.89%</b>

Follow-up 0.0354±0.0008

0.0344±0.0018

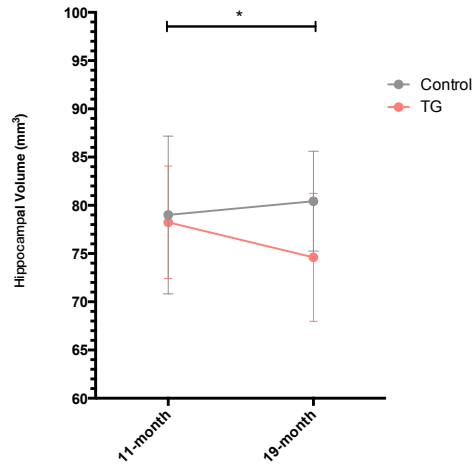
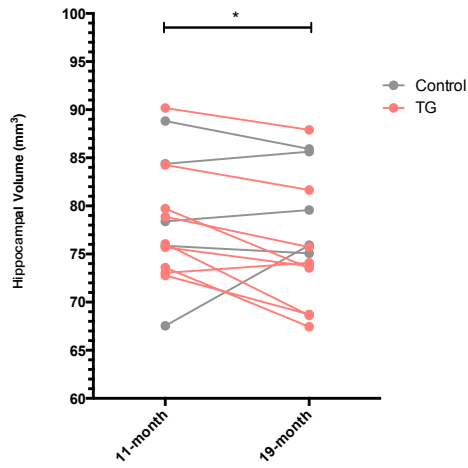
2.82%

Difference 1.67% (ns)

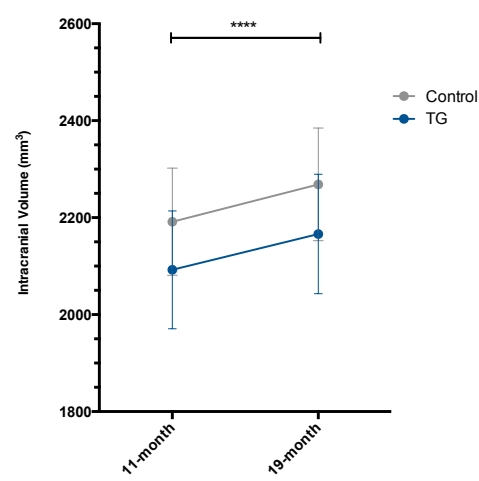
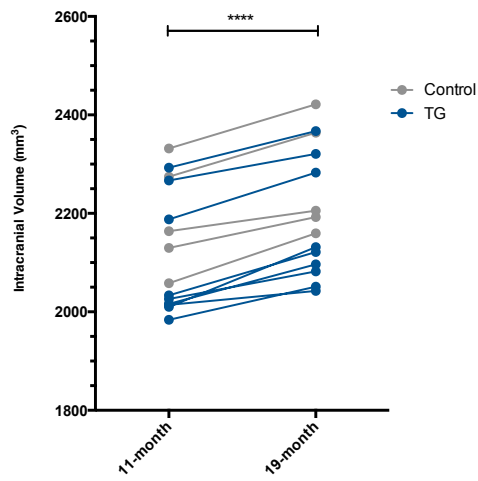
8.02%\*\*\*

(BS>FU)

A)



B)



C)

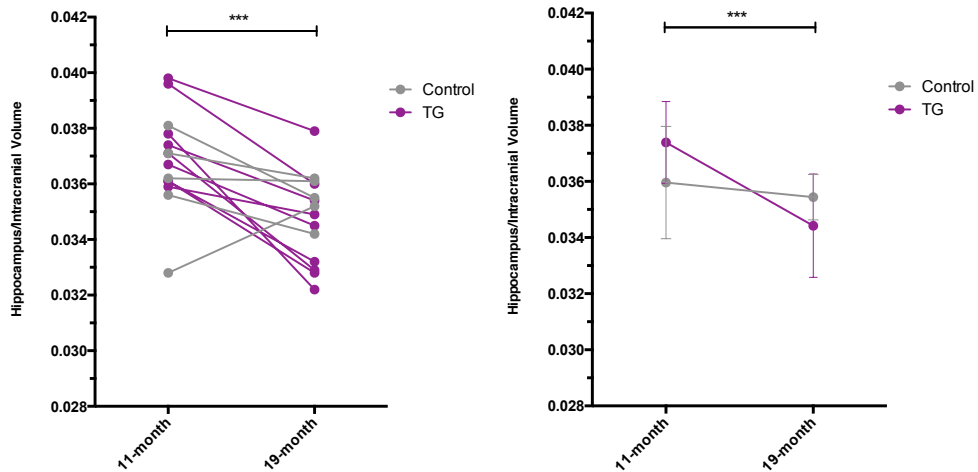


Figure 7. Group comparisons showing an age-dependent A) reduction in hippocampal volume in the Tg group ( $p=0.0164^*$ ), B) increase in intracranial volume of both groups ( $p<0.0001^{****}$ ), C) reduction in normalized hippocampal volume in Tg group ( $p=0.0162^{***}$ ).

### Data Reproducibility

After repeated the manual segmentation procedure 3 times per rat, calculated intra-class correlation coefficient was 0.952.

## Summary and Significance of the Research

### *Summary of Correlation Analysis*

Our results indicate that the amount of both amyloidosis and hypometabolism in pre-symptomatic stages of McGill-R-Thy1-APP rats are able to detect future atrophic patterns that are absent in Wt rats. The degeneration seen in the entorhinal cortex mirrors previous findings that it is indeed an area prone to experience atrophy in correlation with amyloid load in AD (54). Neurodegeneration shown with hypometabolism correlation found in our research, along with ventricular expansion, further confirms human findings of functional disruption contribution to distant atrophy pattern in AD (55). Volume loss in AD hallmark regions in the Tg rats, including the entorhinal cortex, hippocampus, somatosensory cortex, and the insular cortex, confirms that the central role of amyloid resides in the pathogenesis of AD.

### *Summary of Volumetry Analysis*

The hippocampus is amongst one of the first brain regions known to be susceptible to atrophy (27). Our results showing reduction in hippocampal volumes in 19-month old McGill-R-Thy1-APP Tg rats, is consistent with the findings in human studies that A $\beta$  deposition may be sufficient for atrophy in the hippocampus (56). Further investigations of other AD signature regions might provide additional knowledge, since it is suspected that other regions, such as cortical thinning, are related to tau pathology, emphasizing the synergistic mediation of both A $\beta$  and tau on the spatially distinct neurodegenerative patterns in AD (56).

Although our rat model has been validated to display a comparable pattern of plaque distribution as early phases of human AD patients, previous research has been unsuccessful in detecting neuronal loss in the hippocampal and parahippocampal regions of these rats, except for in the subiculum at 19-month old cohort (57). This leads to the potential interpretation that neurodegeneration of hippocampus is occurring at the level of synapses instead of neuronal loss, possibly since at month-19 follow-up, the rats are only approximately 60 years in human.

Maintenance of healthy synapses in our brain is crucial, since synapses are the structures that provide connections between two neurons that work to transmit, process and store information. Factors that are harmful in normal synaptic function, such as A $\beta$  plaques that disturb synaptic mitochondrial function (58) and protein measures (59, 60), diffusible A $\beta$  oligomers (61, 62) that disrupt synaptic plasticity (63) and decrease in long-term potentiation (64), and aging that increases oxidation of synaptic mitochondria (65), may expose AD brains to neurodegeneration. In order to acquire a full understanding of AD pathogenesis, it is important to know the changes occurring at the level of synapses; previous findings have shown A $\beta$ -induced synaptic changes in AD (66), occurring at a very early stage of the disease, prior to detectable NFT (67). Synaptic depletions arise not only as a result of

neuronal death, since still living neurons also lose their synapses in AD (68). More in-depth studies of synaptic disruption in AD revealed regional loss of post-synaptic dendritic material, focusing at the terminal portion of the dendritic tree. Possible explanations of this finding are due to reduced synaptic vesicle trafficking (Coleman and Yao 2003; Synaptic slaughter in AD) or age-dependent accumulation of A $\beta$  and mitochondrial alterations of synaptic mitochondria, making them more susceptible to A $\beta$ -induced damage (58. 62).

It has already been studied in humans that synaptic loss contributes to decline in cognition (61) and that, specifically, synaptic loss of the hippocampus and the neocortex is an early event (69) that correlates with cognitive dysfunction (70). Future studies correlating atrophy patterns with cognitive dysfunction will provide additional information mapping out the pathogenesis of the AD rat model.

### *Validity and Significance of Methodology*

MRI alone is not sufficient to serve as a diagnostic tool of AD, but it provides complementary information, which makes the diagnosis more accurate than using a single modality. One may argue that manual segmentation is a labour-intensive method with a possibility of inter-rater variability, due to subjectivity for definition of structural boundaries (71). However, there are cases when it is a preferred method of quantifying volume changes over automated methods. Automated quantification method, the voxel-wise deformation-based morphometry technique, may be adequate to analyze the whole-brain morphological differences. However, in cases regarding analysis of the volume change of a small region with large surface area-to-volume ratios, manual segmentation method is preferred due possible deviations of the shape or relative anatomical positioning of that region inside the brain (71). Indeed, our correlation coefficient of 0.952 confirmed the validity of the method. Since hippocampal atrophy is not only seen in AD but also in other degenerative diseases (72), manual segmentation quantification method may have applicable roles in providing information for diagnosis of numerous diseases.

### *Limitations and Improvements*

Many challenges exist when conducting research on animal models representative of human diseases. Though inherent to any animal study, one standout limitation of our study is the number of animals used. Several rats were either found dead or developed tumours in different parts of the body, leading to the reduction of power of our analysis.

Another limitation originates from differences in rat development with humans, which needs more attention when working in translational research fields. Instead of the atrophy of the whole brain seen in human AD subjects (28, 73), the rats displayed a growth of the intracranial volume, which was also found to be present in mouse brains, which enlarge significantly from 6-14 months (74). Also, there is a complexity when correlating ages of two very different mammals, and only a very limited number of literature exists regarding this concern. This difficulty is magnified by the fact that the aging processes of mammals are not comparable. For example, rats are sexually mature at 1 month post-natal, which does not adequately compare to a 13-year old human.

Lastly, there is only 1 follow-up in our study. AD is a progressive disease that spans over decades with dynamic pathologies throughout the manifestation. Along with other biomarkers, atrophic pattern was previously found to have a sigmoidal rate (24). Therefore, depending on the time points chosen, hippocampal atrophy rate may or may not be visible. It is important that researchers study the complete developmental process of the disease, rather than focusing on one phase, in order to fully understand the disease characteristic.

### *Future Directions*

In humans, significant reduction in hippocampal volume is known to be observed very early, even years before cognitive symptoms, with increasing rates over time (28). Consequently, volumetric analysis of the Tg rats at a time point earlier than 19

months is needed to identify the exact onset of hippocampal neurodegeneration. Applying longitudinal high-resolution imaging techniques in quantifying regional volume could help distinguish patients that will subsequently develop AD, since it is crucial that neurodegenerations due to aging and AD need to be clearly identified (75). Since mild cognitively impaired subjects with higher level of AB was found to have higher rate of hippocampal atrophy, combination of volumetric information with other biomarkers will provide a more accurate diagnostic tool. Analysis of other AD hallmark areas of neurodegeneration, such as the precuneus and the posterior cingulate (71), may help in providing more information on progressive atrophy pattern.

Further pathological studies are needed to understand the changes occurring at cellular level, including alterations of not only neuronal bodies but also inter-neuronal synaptic areas. By identifying the specific proteomic or cytoskeletal changes occurring in AD brains, therapeutic interventions attempting to block these deteriorations can be studied. Application of this method can be combined with automated segmentation method to develop a semi-automated method that would overcome the challenges of both automated and manual methods.

## References

1. Nilsen, Linn H., Torun M. Melø, Oddbjørn Sæther, Menno P. Witter, and Ursula Sonnewald. "Altered neurochemical profile in the McGill-R-Thy1-APP rat model of Alzheimer's disease: a longitudinal in vivo 1H MRS study." *Journal of neurochemistry* 123, no. 4 (2012): 532-541.
2. Terry, Robert D., Eliezer Masliah, David P. Salmon, Nelson Butters, Richard DeTeresa, Robert Hill, Lawrence A. Hansen, and Robert Katzman. "Physical basis of cognitive alterations in Alzheimer's disease: synapse loss is the major correlate of cognitive impairment." *Annals of neurology* 30, no. 4 (1991): 572-580.
3. Selkoe, Dennis J. "The molecular pathology of Alzheimer's disease." *Neuron* 6, no. 4 (1991): 487-498.

4. Hyman, Bradley T., Gary W. Van Hoesen, Antonio R. Damasio, and Clifford L. Barnes. "Alzheimer's disease: cell-specific pathology isolates the hippocampal formation." *Science* 225, no. 4667 (1984): 1168-1170.
5. IHARA, Yasuo, Nobuyuki NUKINA, Reiko MIURA, and Midori OGAWARA. "Phosphorylated tau protein is integrated into paired helical filaments in Alzheimer's disease." *Journal of biochemistry* 99, no. 6 (1986): 1807-1810.
6. Mortimer, J. A., C. M. Van Duijn, V. Chandra, Laura Fratiglioni, A. B. Graves, A. Heyman, A. F. Jorm et al. "Head trauma as a risk factor for Alzheimer's disease: a collaborative re-analysis of case-control studies." *International journal of epidemiology* 20, no. Supplement 2 (1991): S28-S35.
7. Maheswaran, Satheesh, Hervé Barjat, Daniel Rueckert, Simon T. Bate, David R. Howlett, Lorna Tilling, Sean C. Smart et al. "Longitudinal regional brain volume changes quantified in normal aging and Alzheimer's APP $\times$  PS1 mice using MRI." *Brain research* 1270 (2009): 19-32.
8. Stein, Thor D., and Jeffrey A. Johnson. "Lack of neurodegeneration in transgenic mice overexpressing mutant amyloid precursor protein is associated with increased levels of transthyretin and the activation of cell survival pathways." *The Journal of neuroscience* 22, no. 17 (2002): 7380-7388.
9. Kang, Jie, Hans-Georg Lemaire, Axel Unterbeck, J. Michael Salbaum, Colin L. Masters, Karl-Heinz Grzeschik, Gerd Multhaup, Konrad Beyreuther, and Benno Müller-Hill. "The precursor of Alzheimer's disease amyloid A4 protein resembles a cell-surface receptor." (1987): 733-736.
10. Suzuki, Nobuhiro, Tobun T. Cheung, Xe Dm Cai, Asano Odaka, Laszlo Otvos Jr, Christopher Eckman, Todd E. Golde, and Steven G. Younkin. "An increased percentage of long amyloid beta protein secreted by familial amyloid beta protein precursor (beta APP717) mutants." *Science* 264, no. 5163 (1994): 1336-1340.
11. Ashall, Frank, and Alison M. Goate. "Role of the  $\beta$ -amyloid precursor protein in Alzheimer's disease." *Trends in biochemical sciences* 19, no. 1 (1994): 42-46.
12. Dubois, Bruno, Howard H. Feldman, Claudia Jacova, Steven T. DeKosky, Pascale Barberger-Gateau, Jeffrey Cummings, André Delacourte et al. "Research criteria for the diagnosis of Alzheimer's disease: revising the NINCDS-ADRDA criteria." *The Lancet Neurology* 6, no. 8 (2007): 734-746.

13. Kester, M. I., A. E. Van der Vlies, M. A. Blankenstein, Y. A. L. Pijnenburg, E. J. Van Elk, P. Scheltens, and W. M. van der Flier. "CSF biomarkers predict rate of cognitive decline in Alzheimer disease." *Neurology* 73, no. 17 (2009): 1353-1358.
14. Hansson, Oskar, Henrik Zetterberg, Peder Buchhave, Elisabet Londos, Kaj Blennow, and Lennart Minthon. "Association between CSF biomarkers and incipient Alzheimer's disease in patients with mild cognitive impairment: a follow-up study." *The Lancet Neurology* 5, no. 3 (2006): 228-234.
15. Jack Jr, Clifford R., David S. Knopman, William J. Jagust, Leslie M. Shaw, Paul S. Aisen, Michael W. Weiner, Ronald C. Petersen, and John Q. Trojanowski. "Hypothetical model of dynamic biomarkers of the Alzheimer's pathological cascade." *The Lancet Neurology* 9, no. 1 (2010): 119-128.
16. Bourgeat, Pierrick, Gael Chetelat, V. L. Villemagne, Jurgen Fripp, Parnesh Raniga, K. Pike, Oscar Acosta et al. " $\beta$ -Amyloid burden in the temporal neocortex is related to hippocampal atrophy in elderly subjects without dementia." *Neurology* 74, no. 2 (2010): 121-127.
17. Rowe, Christopher C., and Victor L. Villemagne. "Brain amyloid imaging." *Journal of nuclear medicine technology* 41, no. 1 (2013): 11-18.
18. Morbelli, Silvia, Arnaldo Piccardo, Giampiero Villavecchia, Barbara Dessi, Andrea Brugnolo, Alessandra Piccini, Anna Caroli, Giovanni Frisoni, Guido Rodriguez, and Flavio Nobili. "Mapping brain morphological and functional conversion patterns in amnesic MCI: a voxel-based MRI and FDG-PET study." *European journal of nuclear medicine and molecular imaging* 37, no. 1 (2010): 36-45.
19. Villain, Nicolas, Marine Fouquet, Jean-Claude Baron, Florence Mézenge, Brigitte Landeau, Vincent de La Sayette, Fausto Viader, Francis Eustache, Béatrice Desgranges, and Gaël Chételat. "Sequential relationships between grey matter and white matter atrophy and brain metabolic abnormalities in early Alzheimer's disease." *Brain* 133, no. 11 (2010): 3301-3314.
20. Jack, C. R., M. M. Shiung, J. L. Gunter, P. C. O'Brien, S. D. Weigand, D. S. Knopman, B. F. Boeve et al. "Comparison of different MRI brain atrophy rate measures with clinical disease progression in AD." *Neurology* 62, no. 4 (2004): 591-600.
21. Fox, Nick C., Peter A. Freeborough, and Martin N. Rossor. "Visualisation and quantification of rates of atrophy in Alzheimer's disease." *The Lancet* 348, no. 9020 (1996): 94-97.

22. Schuff, N., N. Woerner, L. Boreta, T. Kornfield, L. M. Shaw, J. Q. Trojanowski, P. M. Thompson, C. R. Jack, and M. W. Weiner. "MRI of hippocampal volume loss in early Alzheimer's disease in relation to ApoE genotype and biomarkers." *Brain* 132, no. 4 (2009): 1067-1077.
23. Leung, Kelvin K., Jonathan W. Bartlett, Josephine Barnes, Emily N. Manning, Sebastien Ourselin, and Nick C. Fox. "Cerebral atrophy in mild cognitive impairment and Alzheimer disease Rates and acceleration." *Neurology* 80, no. 7 (2013): 648-654.
24. Sabuncu, Mert R., Rahul S. Desikan, Jorge Sepulcre, Boon Thye T. Yeo, Hesheng Liu, Nicholas J. Schmansky, Martin Reuter et al. "The dynamics of cortical and hippocampal atrophy in Alzheimer disease." *Archives of neurology* 68, no. 8 (2011): 1040-1048.
25. Dickerson, Bradford C., I. Goncharova, M. P. Sullivan, C. Forchetti, R. S. Wilson, D. A. Bennett, L. A. Beckett, and L. deToledo-Morrell. "MRI-derived entorhinal and hippocampal atrophy in incipient and very mild Alzheimer's disease." *Neurobiology of aging* 22, no. 5 (2001): 747-754.
26. Villain, Nicolas, Marine Fouquet, Jean-Claude Baron, Florence Mézenge, Brigitte Landeau, Vincent de La Sayette, Fausto Viader, Francis Eustache, Béatrice Desgranges, and Gaël Chételat. "Sequential relationships between grey matter and white matter atrophy and brain metabolic abnormalities in early Alzheimer's disease." *Brain* 133, no. 11 (2010): 3301-3314.
27. Fox, N. C., E. K. Warrington, P. A. Freeborough, P. Hartikainen, A. M. Kennedy, J. M. Stevens, and Martin N. Rossor. "Presymptomatic hippocampal atrophy in Alzheimer's disease A longitudinal MRI study." *Brain* 119, no. 6 (1996): 2001-2007.
28. Ridha, Basil H., Josephine Barnes, Jonathan W. Bartlett, Alison Godbolt, Tracey Pepple, Martin N. Rossor, and Nick C. Fox. "Tracking atrophy progression in familial Alzheimer's disease: a serial MRI study." *The Lancet Neurology* 5, no. 10 (2006): 828-834.
29. Knight, W. D., L. G. Kim, A. Douiri, C. Frost, M. N. Rossor, and N. C. Fox. "Acceleration of cortical thinning in familial Alzheimer's disease." *Neurobiology of aging* 32, no. 10 (2011): 1765-1773.
30. Apostolova, Liana G., Kristy S. Hwang, Luis D. Medina, Amity E. Green, Meredith N. Braskie, Rebecca A. Dutton, Jeffrey Lai et al. "Cortical and hippocampal atrophy in patients with autosomal dominant familial Alzheimer's disease." *Dementia and geriatric cognitive disorders* 32, no. 2 (2011): 118-125.

31. De Leon, Mony], AjaxE George, LeonidasA Stylopoulos, Gwenn Smith, and DouglasC Miller. "Early marker for Alzheimer's disease: the atrophic hippocampus." *The Lancet* 334, no. 8664 (1989): 672-673.
32. Jack, C. R., Ronald C. Petersen, Yue Cheng Xu, Peter C. O'Brien, Glenn E. Smith, Robert J. Ivnik, Bradley F. Boeve, Stephen C. Waring, Eric G. Tangalos, and Emre Kokmen. "Prediction of AD with MRI-based hippocampal volume in mild cognitive impairment." *Neurology* 52, no. 7 (1999): 1397-1397.
33. Driscoll, I., C. Davatzikos, Y. An, X. Wu, D. Shen, M. Kraut, and S. M. Resnick. "Longitudinal pattern of regional brain volume change differentiates normal aging from MCI." *Neurology* 72, no. 22 (2009): 1906-1913.
34. Risacher, Shannon L., Andrew J. Saykin, John D. West, Li Shen, Hiram A. Firpi, Brenna C. McDonald, and Alzheimer's Disease Neuroimaging Initiative (ADNI). "Baseline MRI predictors of conversion from MCI to probable AD in the ADNI cohort." *Current Alzheimer Research* 6, no. 4 (2009): 347.
35. Coleman, Paul D., and Dorothy G. Flood. "Neuron numbers and dendritic extent in normal aging and Alzheimer's disease." *Neurobiology of aging* 8, no. 6 (1987): 521-545.
36. Ball, M. J., V. Hachinski, A. Fox, A. J. Kirshen, M. Fisman, W. Blume, V. A. Kral, H. Fox, and H. Merskey. "A new definition of Alzheimer's disease: a hippocampal dementia." *The Lancet* 325, no. 8419 (1985): 14-16.
37. Hardy, John A., and Gerald A. Higgins. "Alzheimer's disease: the amyloid cascade hypothesis." *Science* (1992).
38. Hardy, John, and Dennis J. Selkoe. "The amyloid hypothesis of Alzheimer's disease: progress and problems on the road to therapeutics." *Science* 297, no. 5580 (2002): 353-356.
39. Baudier, J., and R. David Cole. "Phosphorylation of tau proteins to a state like that in Alzheimer's brain is catalyzed by a calcium/calmodulin-dependent kinase and modulated by phospholipids." *Journal of Biological Chemistry* 262, no. 36 (1987): 17577-17583.
40. Jack Jr, Clifford R., David S. Knopman, William J. Jagust, Ronald C. Petersen, Michael W. Weiner, Paul S. Aisen, Leslie M. Shaw et al. "Tracking pathophysiological processes in Alzheimer's disease: an updated hypothetical model of dynamic biomarkers." *The Lancet Neurology* 12, no. 2 (2013): 207-216.
41. McKhann, Guy, David Drachman, Marshall Folstein, Robert Katzman, Donald Price, and Emanuel M. Stadlan. "Clinical diagnosis of Alzheimer's disease

- Report of the NINCDS-ADRDA Work Group\* under the auspices of Department of Health and Human Services Task Force on Alzheimer's Disease." *Neurology* 34, no. 7 (1984): 939-939.
42. Laakso, M. P., H. Soininen, K. Partanen, E-L. Helkala, P. Hartikainen, P. Vainio, M. Hallikainen, T. Hänninen, and P. J. Riekkinen Sr. "Volumes of hippocampus, amygdala and frontal lobes in the MRI-based diagnosis of early Alzheimer's disease: correlation with memory functions." *Journal of Neural Transmission-Parkinson's Disease and Dementia Section 9*, no. 1 (1995): 73-86.
  43. Scheltens, P., F. Pasquier, J. G. E. Weerts, F. Barkhof, and D. Leys. "Qualitative assessment of cerebral atrophy on MRI: inter-and intra-observer reproducibility in dementia and normal aging." *European neurology* 37, no. 2 (1997): 95-99.
  44. Cuénod, Charles-André, Alban Denys, Jean-Luc Michot, Philippe Jehenson, Françoise Forette, David Kaplan, André Syrota, and François Boller. "Amygdala atrophy in Alzheimer's disease: an in vivo magnetic resonance imaging study." *Archives of Neurology* 50, no. 9 (1993): 941-945.
  45. Erkinjuntti, Timo, Donald H. Lee, Fuqiang Gao, Runa Steenhuis, Michael Eliasziw, Rick Fry, Harold Merskey, and Vladimir C. Hachinski. "Temporal lobe atrophy on magnetic resonance imaging in the diagnosis of early Alzheimer's disease." *Archives of Neurology* 50, no. 3 (1993): 305-310.
  46. Laakso, M. P., Kaarina Partanen, P. Riekkinen, Maarit Lehtovirta, E-L. Helkala, Merja Hallikainen, Tuomo Hanninen, Paula Vainio, and Hilikka Soininen. "Hippocampal volumes in Alzheimer's disease, Parkinson's disease with and without dementia, and in vascular dementia An MRI study." *Neurology* 46, no. 3 (1996): 678-681.
  47. Tien, R. D., G. J. Felsberg, and J. MacFall. "Practical choices of fast spin echo pulse sequence parameters: clinically useful proton density and T2-weighted contrasts." *Neuroradiology* 35, no. 1 (1992): 38-41.
  48. Davatzikos, Christos, Yong Fan, Xiaoying Wu, Dinggang Shen, and Susan M. Resnick. "Detection of prodromal Alzheimer's disease via pattern classification of magnetic resonance imaging." *Neurobiology of aging* 29, no. 4 (2008): 514-523.
  49. Gaser, Christian, Igor Nenadic, Bradley R. Buchsbaum, Erin A. Hazlett, and Monte S. Buchsbaum. "Deformation-based morphometry and its relation to conventional volumetry of brain lateral ventricles in MRI." *Neuroimage* 13, no. 6 (2001): 1140-1145.

50. Ashburner, John, and Karl J. Friston. "Voxel-based morphometry—the methods." *Neuroimage* 11, no. 6 (2000): 805-821.
51. Higgins, Guy A., and Heimit Jacobsen. "Transgenic mouse models of Alzheimer's disease: phenotype and application." *Behavioural pharmacology* 14, no. 5-6 (2003): 419-438.
52. Tesson, Laurent, Jean Cozzi, Severine Menoret, Severine Remy, Claire Usal, Alexandre Fraichard, and Ignacio Anegón. "Transgenic modifications of the rat genome." *Transgenic research* 14, no. 5 (2005): 531-546.
53. Leon, Wanda Carolina, Fabio Canneva, Vanessa Partridge, Simon Allard, Maria Teresa Ferretti, Arald DeWilde, Freya Vercauteren et al. "A Novel Transgenic Rat Model with a Full Alzheimer's-Like Amyloid Pathology Displays Pre-Plaque Intracellular Amyloid- $\beta$ -Associated Cognitive Impairment." *Journal of Alzheimer's Disease* 20, no. 1 (2010): 113-126.
54. Archer, Hilary A., Paul Edison, David J. Brooks, Jo Barnes, Chris Frost, Tom Yeatman, Nick C. Fox, and Martin N. Rossor. "Amyloid load and cerebral atrophy in Alzheimer's disease: An 11C-PIB positron emission tomography study." *Annals of neurology* 60, no. 1 (2006): 145-147.
55. Chételat, G., B. Desgranges, B. Landeau, F. Mézenge, J. B. Poline, V. De La Sayette, F. Viader, F. Eustache, and J-C. Baron. "Direct voxel-based comparison between grey matter hypometabolism and atrophy in Alzheimer's disease." *Brain* 131, no. 1 (2008): 60-71.
56. Wang, Liang, Tammie L. Benzinger, Jason Hassenstab, Tyler Blazey, Christopher Owen, Jingxia Liu, Anne M. Fagan, John C. Morris, and Beau M. Ances. "Spatially distinct atrophy is linked to  $\beta$ -amyloid and tau in preclinical Alzheimer disease." *Neurology* 84, no. 12 (2015): 1254-1260.
57. Heggland, Ingrid, Inge S. Storakaas, Hanne T. Soligard, Asgeir Kobro-Flatmoen, and Menno P. Witter. "Stereological estimation of neuron number and plaque load in the hippocampal region of a transgenic rat model of Alzheimer's disease." *European Journal of Neuroscience* 41, no. 9 (2015): 1245-1262.
58. Du, Heng, Lan Guo, Shiqiang Yan, Alexander A. Sosunov, Guy M. McKhann, and Shirley ShiDu Yan. "Early deficits in synaptic mitochondria in an Alzheimer's disease mouse model." *Proceedings of the National Academy of Sciences* 107, no. 43 (2010): 18670-18675.
59. Lassmann, H., R. Weiler, P. Fischer, C. Bancher, K. Jellinger, E. Floor, W. Danielczyk, F. Seitelberger, and H. Winkler. "Synaptic pathology in Alzheimer's disease: immunological data for markers of synaptic and large dense-core vesicles." *Neuroscience* 46, no. 1 (1992): 1-8.

60. Sze, Chun-I., Juan C. Troncoso, Claudia Kawas, PETER MOUTION, Donald L. Price, and Lee J. Martin. "Loss of the presynaptic vesicle protein synaptophysin in hippocampus correlates with cognitive decline in Alzheimer disease." *Journal of Neuropathology & Experimental Neurology* 56, no. 8 (1997): 933-944.
61. Arendt, Thomas. "Synaptic degeneration in Alzheimer's disease." *Acta neuropathologica* 118, no. 1 (2009): 167-179.
62. Reddy, P. Hemachandra, and M. Flint Beal. "Amyloid beta, mitochondrial dysfunction and synaptic damage: implications for cognitive decline in aging and Alzheimer's disease." *Trends in molecular medicine* 14, no. 2 (2008): 45-53.
63. Lacor, Pascale N., Maria C. Buniel, Paul W. Furlow, Antonio Sanz Clemente, Pauline T. Velasco, Margaret Wood, Kirsten L. Viola, and William L. Klein. "A $\beta$  oligomer-induced aberrations in synapse composition, shape, and density provide a molecular basis for loss of connectivity in Alzheimer's disease." *The Journal of neuroscience* 27, no. 4 (2007): 796-807.
64. Townsend, Matthew, Ganesh M. Shankar, Tapan Mehta, Dominic M. Walsh, and Dennis J. Selkoe. "Effects of secreted oligomers of amyloid  $\beta$ -protein on hippocampal synaptic plasticity: a potent role for trimers." *The Journal of physiology* 572, no. 2 (2006): 477-492.
65. Martinez, Marcos, Ana Isabel Hernández, Natividad Martínez, and María Luisa Ferrándiz. "Age-related increase in oxidized proteins in mouse synaptic mitochondria." *Brain research* 731, no. 1 (1996): 246-248.
66. Haass, Christian, and Dennis J. Selkoe. "Soluble protein oligomers in neurodegeneration: lessons from the Alzheimer's amyloid  $\beta$ -peptide." *Nature reviews Molecular cell biology* 8, no. 2 (2007): 101-112.
67. Coleman, Paul, Howard Federoff, and Roger Kurlan. "A focus on the synapse for neuroprotection in Alzheimer disease and other dementias." *Neurology* 63, no. 7 (2004): 1155-1162.
68. Coleman, Paul D., and Pamela J. Yao. "Synaptic slaughter in Alzheimer's disease." *Neurobiology of aging* 24, no. 8 (2003): 1023-1027.
69. Heinonen, O., H. Soininen, H. Sorvari, O. Kosunen, L. Palja, E. Koivisto, and P. J. Riekkinen. "Loss of synaptophysin-like immunoreactivity in the hippocampal formation is an early phenomenon in Alzheimer's disease." *Neuroscience* 64, no. 2 (1995): 375-384.

70. Masliah, E. "Mechanisms of synaptic dysfunction in Alzheimer's disease." (1995).
71. Scahill, Rachael I., Jonathan M. Schott, John M. Stevens, Martin N. Rossor, and Nick C. Fox. "Mapping the evolution of regional atrophy in Alzheimer's disease: unbiased analysis of fluid-registered serial MRI." *Proceedings of the National Academy of Sciences* 99, no. 7 (2002): 4703-4707.
72. Jack, C. R., D. W. Dickson, J. E. Parisi, Y. C. Xu, R. H. Cha, P. C. O'Brien, S. D. Edland et al. "Antemortem MRI findings correlate with hippocampal neuropathology in typical aging and dementia." *Neurology* 58, no. 5 (2002): 750-757.
73. Dickerson, Bradford C., Akram Bakkour, David H. Salat, Eric Feczko, Jenni Pacheco, Douglas N. Greve, Fran Grodstein et al. "The cortical signature of Alzheimer's disease: regionally specific cortical thinning relates to symptom severity in very mild to mild AD dementia and is detectable in asymptomatic amyloid-positive individuals." *Cerebral cortex* 19, no. 3 (2009): 497-510.
74. Maheswaran, Satheesh, Hervé Barjat, Daniel Rueckert, Simon T. Bate, David R. Howlett, Lorna Tilling, Sean C. Smart et al. "Longitudinal regional brain volume changes quantified in normal aging and Alzheimer's APP $\times$  PS1 mice using MRI." *Brain research* 1270 (2009): 19-32.
75. Perrin, Richard J., Anne M. Fagan, and David M. Holtzman. "Multimodal techniques for diagnosis and prognosis of Alzheimer's disease." *Nature* 461, no. 7266 (2009): 916-922.